Marine and Petroleum Geology
July 2019, Volume 105, Pages 185-203
https://doi.org/10.1016/j.marpetgeo.2019.04.009
https://archimer.ifremer.fr/doc/00489/60066/

Neogene evolution and demise of the Amapá carbonate platform, Amazon continental margin, Brazil

Cruz A.M. [1, *], Reis A.T. [2], Suc J.P. [1], Silva C.G. [3], Praeg D. [3, 4, 5], Granjeon D. [6], Rabineau Marina [7], Popescu S.M. [8], Gorini C. [1]

[1] Sorbonne Université, CNRS-INSU, Institut des Sciences de la Terre Paris, ISTeP UMR 7193, 75005, Paris, France
[2] Department of Geological Oceanography, School of Oceanography, Rio de Janeiro State University (UERJ), Rua São Francisco Xavier, 524, 4° Andar, Bl. E, Maracanã, Rio de Janeiro/RJ, CEP: 20.550-013, Brazil
[3] Departamento de Geologia-Lagemar, Universidade Federal Fluminense (UFF), Av. Litorânea, s/n, Boa Viagem, Niterói, RJ, CEP: 24210-346, Brazil
[4] Institute of Petroleum and Natural Resources, Pontifícia Universidade Católica do Rio Grande do Sul – PUCRS, Av. Ipiranga, 6681, Porto Alegre, Brazil
[5] Géoazur, UMR7329 CNRS, 250 Rue Albert Einstein, 06560, Valbonne, France
[6] IFP Energies Nouvelles, 1-4 avenue de Bois-Préau, 92852, Rueil-Malmaison, France
[7] Institut Français de Recherche pour l'Exploitation de la Mer (IFREMER), DRO/GM/LGG, BP 70, 29280, Plouzané, France
[8] GeoBioStratData Consulting. 385 Route du Mas Rillier, 69140, Rillieux la Pape, France

* Corresponding author : A. M. Cruz, email address : albertocruzgeo@gmail.com

Abstract :

The Amazon continental shelf hosted one of the world's largest mixed carbonate-siliciclastic platforms from the late Paleocene onwards - the Amapá carbonates. The platform architecture, however, remains poorly understood and causes and timing of the cessation of carbonate deposition are still controversial. Here we present a stratigraphic analysis of the Neogene succession of the Amapá carbonates, based on a grid of 2D/3D seismic data correlated to revised micropaleontological data from exploration wells. The results provide improved constraints on the age of the transition from predominantly carbonate to siliciclastic sedimentation, which is shown to have varied through time across three different sectors of the shelf (NW, Central and SE). Four Neogene evolutionary stages of carbonate deposition could be defined and dated with reference to the new age model: (1) between ca. 24 and 8 Ma a predominantly aggrading mixed carbonate-siliciclastic shelf prevailed across the entire region carbonate production gave way to siliciclastic sedimentation across the Central and SE shelves; (2) between 8 and 5.5 Ma carbonate production continued to dominate the NW shelf, as deposition was able to keep up with base level oscillations; (3) between 5.5 and 3.7 Ma (early Pliocene), sediment supply from the paleo-Amazon River promoted the progressive burial of carbonates on the inner NW shelf, while carbonates production continued on the outer shelf (until 3.7 Ma). Longer-lasting carbonate sedimentation on the NW shelf can be explained by a lesser influx of siliciclastic sediments due to the paleo-geography of the Central shelf, characterized by a 150-km-wide embayment, which directed most terrigenous sediments sourced from the paleo-Amazon River to the continental slope and deep ocean; (4) from 3.7 Ma onwards, when the Central shelf embayment became completely filled, continuous sediment supply to the NW shelf

resulted in the final transition from carbonate to siliciclastic-dominated environments on the entire Offshore Amazon Basin.

Highlights

► New age models allow to clarify the Neogene history of the Amazon shelfal carbonates. ► Differential subsidence strongly controls shelf architecture between ca. 24–3,7Ma ► Higher siliciclastic influx suppressed the Central and NW shelf carbonates at ca. 8Ma ► Carbonate production locally persisted on the NW Amazon shelf until ca. 3.7Ma ► Reduction of regional subsidence rates led to the death of shelfal carbonates.

Keywords : Mixed carbonate-siliciclastic platform, carbonate architecture, chonostratigraphic model, non-eustatic accommodation, shelf paleogeography

1. INTRODUCTION

Carbonate units were first reported from commercial well data in the Foz do Amazonas Basin (hereafter Offshore Amazon Basin) by Schaller et al. (1971), who named them the Amapá Formation (hereafter Amapá carbonates). The Amapá carbonates were subsequently shown to comprise a succession of bioaccumulated units up to 4000 m thick (Brandão and Feijó, 1994), considered to be the largest coralgal-foraminiferal platform in the geological record by Carozzi (1981) and Wolff and Carozzi (1984). Analyses of well data showed deposition of the Amapá carbonates to have taken place contemporaneously with siliciclastic sedimentation on the inner continental shelf (Marajó Formation), consisting of proximal fan deltas and lagoonal facies, connected to the open ocean by shelf-transverse troughs filled with shales interbedded with carbonate olistoliths (Schaller et al., 1971; Carozzi, 1981).

Most studies of the Offshore Amazon Basin agree that shelfal carbonate sedimentation started during the Paleocene (Brandão and Feijó, 1994; Figueiredo et al., 2007; Figueiredo et al., 2009). However, estimates of the cessation of carbonate deposition in the basin vary, from middle Miocene to early Pliocene (*e.g.* Schaller et al., 1971; Carozzi, 1981; Figueiredo et al., 2009; Gorini et al., 2014). The origin of the terrigenous sediments that buried the carbonate platform is also disputed, and has a broader importance due to the common assumption that the end of carbonate deposition marked the onset of the transcontinental Amazon River (Schaller et al., 1971; Silva et al., 1999; Figueiredo et al., 2007; Figueiredo et al., 2009). Based on stratigraphic analyses of offshore seismic and well data, the present-day Amazon deep-sea fan (hereafter Amazon fan; Fig.1) is the result of a rapid increase in supply of siliciclastic sediments to the offshore basin around the middle to late Miocene transition, interpreted to record the first appearance of a transcontinental river that connected the Andean Range and the Atlantic Ocean (Castro et al., 1978; Silva et al., 1999; Dobson et al., 2001;

Figueiredo et al., 2007; Figueiredo et al., 2009; Hoorn et al., 2017). However, this hypothesis based on offshore data has been questioned by paleogeographical reconstructions based on studies in onshore Amazonian basins, which consider a transcontinental Amazon River to have first appeared during the late Pliocene-Quaternary (e.g., Campbell et al., 2006; Latrubesse et al., 2010; Nogueira et al., 2013). These paleogeographical models do not envisage a westward enlargement of the paleo-Amazon River catchment basin beyond the Brazilian and Guiana shields prior to the late Pliocene, and so require alternative explanations for the observed increase in offshore terrigenous influx since the late Miocene.

Thus, both the timing and nature of the transition from a carbonate to a siliciclastic-dominated margin offshore the Amazon River remain controversial, and of broad interest for the Neogene paleo-geographic history of this part of South America. The aim of this paper is to better constrain the timing of cessation of carbonate production on the Amazon continental margin in order to understand the mechanisms that controlled the distribution of Neogene carbonate sedimentary units. The results allow us to reconstruct the interaction between carbonate and siliciclastic depositional environments in space and time during several distinct stages in the evolution and progressive burial of the Amapá carbonates. Our findings also allow an assessment of the possible controls on this equatorial carbonate factory in a Neogene context of variable sediment supply from the paleo-Amazon River and sea-level changes of varying amplitude and frequency.

2. REGIONAL GEOLOGICAL SETTING

The Offshore Amazon Basin is located in the northwestern portion of the Brazilian Equatorial Margin (Fig. 1), which was formed during the opening of the Equatorial Atlantic Ocean in a context of wrench tectonics that involved two phases: an early, less intense phase during the Triassic-Jurassic; and a later phase related to continental rifting during the Early Cretaceous (Matos, 2000).

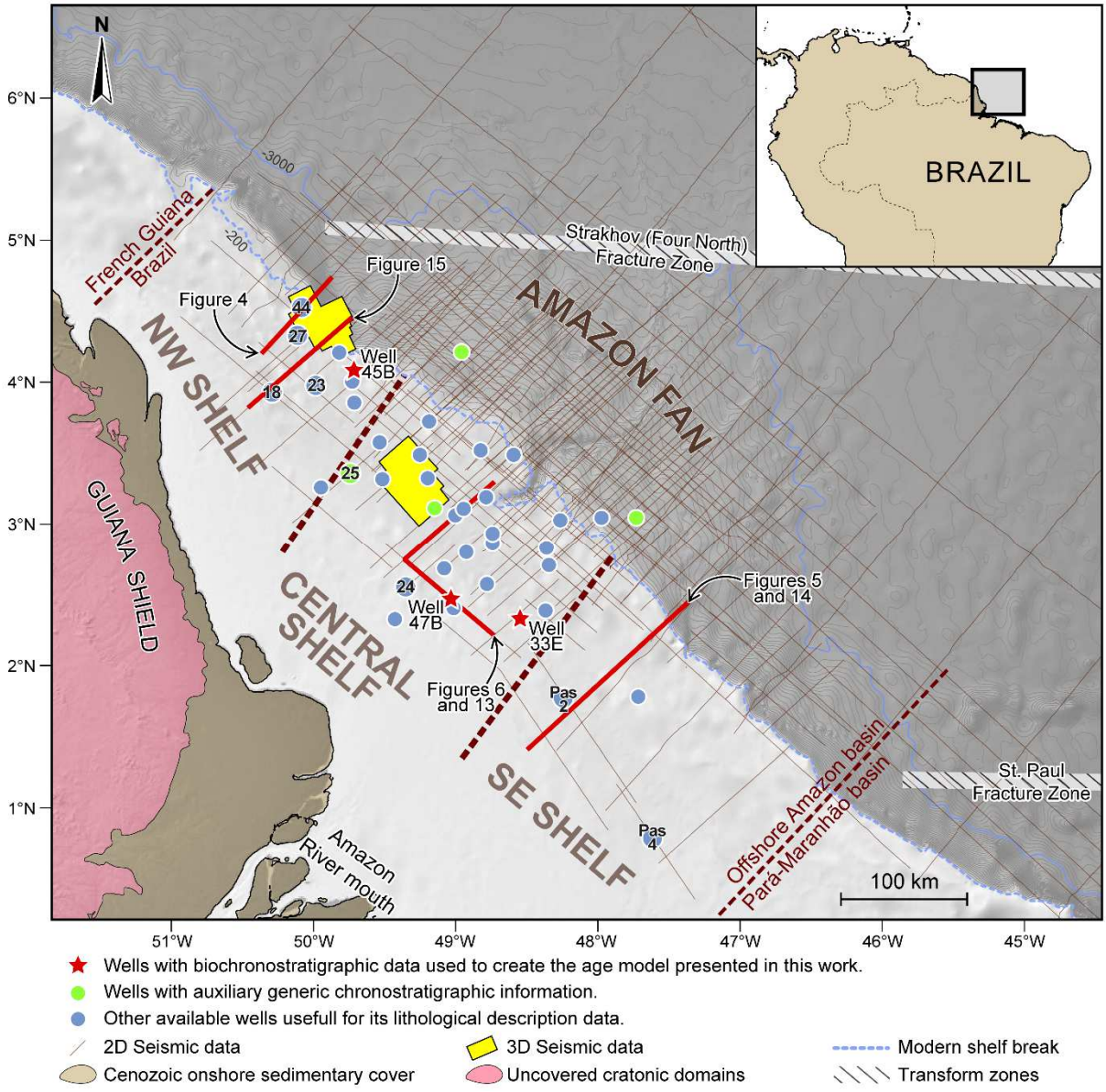

Figure 1: Map of the study area showing the available seismic and well dataset. The Amazon Offshore Basin is subdivided into three regions, shown by thick dashed lines. The locations of Figures 4 to 6 and 13 to15 are shown by red lines.

Within the Offshore Amazon Basin, stratigraphic studies using seismic profiles tied to well data indicate that the Lower Cretaceous rift succession is composed of Neocomian to Albian fluvio-deltaic, lacustrine and marine strata, infilling half-graben of pull-apart basins (Brandão and Feijó, 1994; Figueiredo et al., 2007). Open-marine clastic deposition began during the Albian (ca. 102 Ma; Figueiredo et al., 2007) with the deposition of deep-water mudstones and siltstones and lasted until the Paleocene (Limoeiro Formation; Fig. 2). Most studies agree that from the late Paleocene (ca. 59 Ma; Figueiredo et al., 2007) to the late Miocene, the basin was dominated by mixed carbonate-siliciclastic shelfal sediments (Marajo and Amapá Formations), laterally equivalent to deep-water calcilutites and mudstones (Travosas Formation; Wolff and Carozzi, 1984; Figueiredo et al., 2007; Fig. 2). The Amapá carbonates deposition can be subdivided into four major depositional cycles interrupted by periods of subaerial exposure (Carozzi, 1981; Wolff and Carozzi, 1984): Cycle I (Paleocene to early Eocene); Cycle II (middle Eocene); Cycle III (late Eocene to late Oligocene); Cycle IV (early to middle Miocene). The latter cycle corresponds to the time interval investigated in this study, the youngest age of which is uncertain as discussed below. From the late Miocene onwards, increasing siliciclastic input resulted in prograding shelf clinoforms that ultimately buried the Amapá carbonates (Gorini et al., 2014).

The youngest age of the Amapá carbonates has been repeatedly revised. Early studies placed the cessation of carbonate sedimentation within the middle Miocene (Schaller et al., 1971; Carozzi, 1981) or at the middle to late Miocene boundary (Wolff and Carozzi, 1984; Brandão and Feijó, 1994). Silva et al. (1999) were the first to assign a precise age for the top of the carbonate platform, at 10 Ma. Figueiredo et al. (2009), based on calcareous nannofossil zonations, first assigned an age between 11.8 and 11.3 Ma for the top of the carbonate platform. This age was questioned by Campbell (2010) and revised to 10.5 Ma by Figueiredo

et al. (2010). More recently, based on calcareous nannofossil zonations, Gorini et al. (2014) argued that the end of carbonate sedimentation was not synchronous across the basin, placing the top of the platform between 9.5 and 8.3 Ma on the Central shelf, and younger on the NW shelf although it was not possible to propose a precise age.

The nature of the stratal relationships recording the transition from carbonate to terrigenous sedimentation in the Offshore Amazon Basin is also disputed. Based on well data, Carozzi (1981) proposed that the top of the carbonate platform was marked by a large transgression caused by a sea-level rise. In contrast, also based on well data, Figueiredo et al. (2009) proposed that the same stratigraphic level was marked by a "regional unconformity" associated with the Serravallian/Tortonian eustatic fall highlighted by Haq et al. (1987). More recently, Gorini et al. (2014) used seismic and well data to show that the carbonates are downlapped by shelf clinoforms, supporting an interpretation of the carbonate-siliciclastic boundary as a flooding surface.

Seaward of the shelf, the continental slope is dominated by the lobate form of the Amazon fan (Fig. 1), a vast sedimentary depocenter that is interpreted to record an increase in siliciclastic influx since the late Miocene (Silva et al., 1999). It has been generally assumed that deposition of the Amazon fan began around the same time that carbonate sedimentation on the shelf was suppressed (e.g., Schaller et al., 1971; Silva et al., 1999; Figueiredo et al., 2007; Figueiredo et al., 2009). Based on an extrapolation of latest Quaternary sedimentation rates in cores, Damuth and Kumar (1975) and Damuth et al. (1983) suggested initiation of the Amazon fan between 16.5 and 8 Ma, in the middle to late Miocene. Subsequently, with the aid of correlation of well data to seismic profiles, Silva et al. (1999), Figueiredo et al. (2007) and Figueiredo et al. (2009) proposed ages between 11.8 and 10.5 Ma for the base of the Amazon fan. More recently, Hoorn et al. (2017) proposed an age between 9.4 and 9 Ma for the base of the fan, based on planktonic calcareous nannofossil zonations in a single well,

calibrated to the international time scale of Gradstein et al. (2012). These authors also suggested for the first time that the Amazon fan could post-date the cessation of shelfal carbonate sedimentation by 1 to.5 Myr.

Sedimentation rates in the Offshore Amazon Basin remained relatively low in the late Miocene, with estimated values around 0.05 m/kyr, but increased dramatically during the late Pliocene-Pleistocene to estimated values of 0.34 m/kyr and 1.22 m/kyr on the shelf and in the fan regions, respectively (Figueiredo et al., 2009; Gorini et al., 2014).The corresponding sediment thicknesses (of up to 9 km) promoted isostatic subsidence and flexural deformation of the lithosphere, beneath the fan and adjoining regions (Braga, 1993; Driscoll and Karner, 1994; Silva et al., 1999; Rodger et al., 2006).

The Amazon continental margin has also been strongly affected by two main types of gravity-driven slope processes operating over differing temporal and spatial scales (Reis et al., 2010; Reis et al., 2016). During the Neogene, gravity-driven synsedimentary tectonics resulted in the sliding of thick Cretaceous to Recent sedimentary sequences above multiple levels of basal décollements, to generate a structural system composed of a proximal extensional domain on the outer shelf and upper slope and giving way to a distal compressive domain (thrust-and-fold belts) on the slope above water depths of ~2600 m (Cobbold et al., 2004; Perovano et al., 2009; Reis et al., 2010). The uppermost seismically-detected décollement surface has been interpreted as a condensed section laterally correlative to the top of the Amapá carbonates (Reis et al., 2016). This surface has also acted as a basal décollement (Reis et al., 2016) during a series of large-scale slope failures recorded by a succession of giant mass-transport deposits (MTDs; Silva et al., 2010; Silva et al., 2016; Reis et al., 2016).

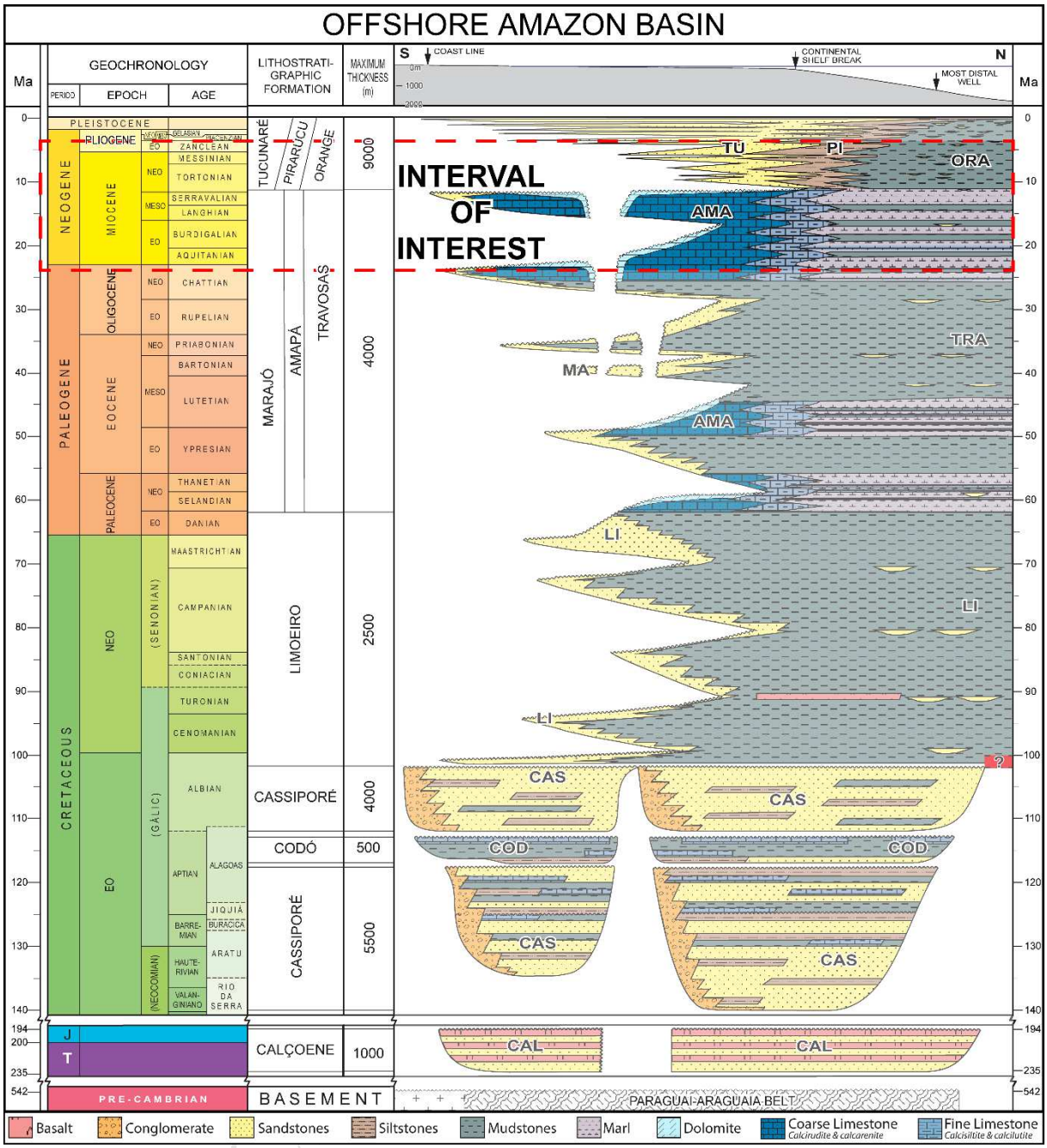

Figure 2: Stratigraphic chart of the Amazon Offshore Basin (simplified from Figueiredo et al., 2007). The dashed red box indicates the interval investigated in this study. Note that, based on confidential biostratigraphic zonations of Petrobras correlated to Gradstein et al. (2004) geochronology, the top of the Amapá carbonates was placed at 10.5 Ma by Figueiredo et al. (2007), while more recent studies have proposed ages varying between 11.8 and 8.3 Ma (see text for details).

3. DATA AND METHODS

The study is based on a shelf-wide grid of multi-channel commercial 2D and 3D seismic reflection data, correlated to biostratigraphic and lithological data from exploration wells (Fig. 1). The seismic dataset includes 20,000 km of 2D seismic profiles and two 3D blocks covering a total area of 3,800 km^2 (Fig.1). The 2D seismic profiles have record lengths of 10-13 seconds, with vertical resolution of 10–50 m (generally decreasing with depth as velocity increases). The data were interpreted following standard seismic-stratigraphic methods, in which reflection relations (onlap, downlap, truncation, conformity) are used to define units bounded by unconformities and correlative conformities or maximum flooding surfaces (e.g. Mitchum and Vail, 1977; Vail et al., 1977; Catuneanu 2006). The unit-bounding surfaces presented in this work can be either unconformities or maximum flooding surfaces; the interpretations are made on the basis of architectural styles and lithological content rather than following a given sequence-stratigraphic concept.

Seismic facies analysis of the internal character of the units was used together with lithological data from wells to identify depositional environments (carbonate vs. siliciclastic dominated) and their variations across the shelf (Schlager, 1998; Pomar, 2001; Schlager, 2005; Burgess et al., 2013). Seismic-stratigraphic analysis is not based on genetic concepts of depositional sequences, but as a means of defining physical units bounded by surfaces that mark major changes in architectural style of carbonates (on seismic data) and lithological content (from well data).

Downhole information on unit lithology was obtained from 40 exploratory wells located across the shelf and upper slope: gamma ray, sonic, and lithological logs in well reports (Fig. 1). Carbonate and siliciclastic units are identified from lithological descriptions on composite logs (based on cuttings and sidewall cores). An age model for these units was constructed through the revision of biostratigraphic information obtained from three wells:

published data from well 33E (Figueiredo et al., 2009), and unpublished reports for wells 45B and 47B (Fig. 1). The first and last occurrences of key calcareous nannoplankton species were used to assign minimum and maximum possible ages to the main stratigraphic surfaces based on published biochronostratigraphic compilations (Martini, 1971; Young, 1998; Raffi et al., 2006; Anthonissen and Ogg, 2012; Zeeden et al., 2013), updated to the astronomically-tuned geologic time scale (Gradstein et al., 2012). Age ranges for unit boundaries were assigned based on their position relative to markers in the wells. More precise ages for each surface were then proposed based on correlation to the global sea-level curves of Miller et al. (2005) and Haq et al. (1987), recalibrated to the timescale of Gradstein et al. (2012). The ages of the sea-level oscillations of Haq et al. (1987) were revised by recalibrating their associated magneto-polarity chrons (time in Ma) to those updated by Gradstein et al. (2012).

In addition, data from seven exploratory wells were used to estimate minimum values of non-eustatic accommodation space creation across the shelf during deposition of the upper Amapá carbonates. Minimum values of non-eustatic accommodation creation were calculated by subtracting the value of maximum eustatic rise reached during the period of deposition of each sedimentary unit, based on published global sea-level curves (Haq et al., 1987; Miller et al., 2005), from the undecompacted thickness of the units at the well sites. As global sea-level curves contain uncertainties in amplitude and cyclicity, our estimates of non-eustatic accommodation space creation were made using the curves of both Haq et al. (1987) and Miller et al. (2005), in order to take into account the full variety of sea-level scenarios available in the literature.

4. **RESULTS**

We first present new information on the stratal architecture of the upper Amapá carbonates, using seismic data correlated to wells (Fig. 1) to characterize the bounding

surfaces and internal seismic facies of five regional units (Figs 3-6) and to map the changing distribution of carbonate- and siliciclastic-dominated environments across the shelf through time (Fig. 7). We then present an age model for the Neogene units, constrained by revised biostratigraphic data from wells (Figs 8-10) and correlated with global curves of sea-level oscillations (Fig. 11). Finally, we present estimates of minimum non-eustatic accommodation space across the shelf through the Neogene (Fig. 12).

4.1. Depositional units and architecture of the upper Amapá carbonates

Based on correlation of interpreted seismic data to lithological information from wells, the upper sedimentary succession of the Amapá carbonates is divided into 5 main stratigraphic units, referred to as N1 to N5 (Figs. 3-6).

Units N1 to N5 discussed below are time equivalent to carbonate deposition cycle IV defined in the same Amazon shelf from well data by Carozzi (1981) and Wolff and Carozzi (1984). These authors described the carbonate depositional environments as being mostly a coralgal platform with banks dominated by “red algae bioconstructed limestones” and subordinated coralline deposits, as well as “broad lagoonal belts rich in bryozoans”. We did not have direct access to samples from the wells used in the present study, precluding a description and analysis of depositional facies. Available well reports provide only general descriptions of either carbonate or siliciclastic lithologies using terms such as calcarenites, calcisiltite, calcilutite, sandstone, siltstone or shale. Thus, the description of units N1 to N5 is presented below in terms of the vertical and lateral distribution of carbonate versus siliciclastic lithological content.

For descriptive purposes, the shelf was divided into three regions: NW shelf, Central shelf and SE shelf (Fig. 1). Units N1 to N5 are less architecturally complex on the NW Shelf, where they are also clearly imaged on seismic data; in contrast, on the Central shelf seismic

imaging is poorer due to a greater thickness of the overlying Pliocene-Quaternary units and the occurrence of complex geometries, gravity-driven synsedimentary tectonic deformations and mass-wasting scars (Figs. 4 and 6). For clarity, in each of the following sections, units N1 to N5 will be described from less to more complex regions: the NW shelf, the SE shelf and finally the Central shelf.

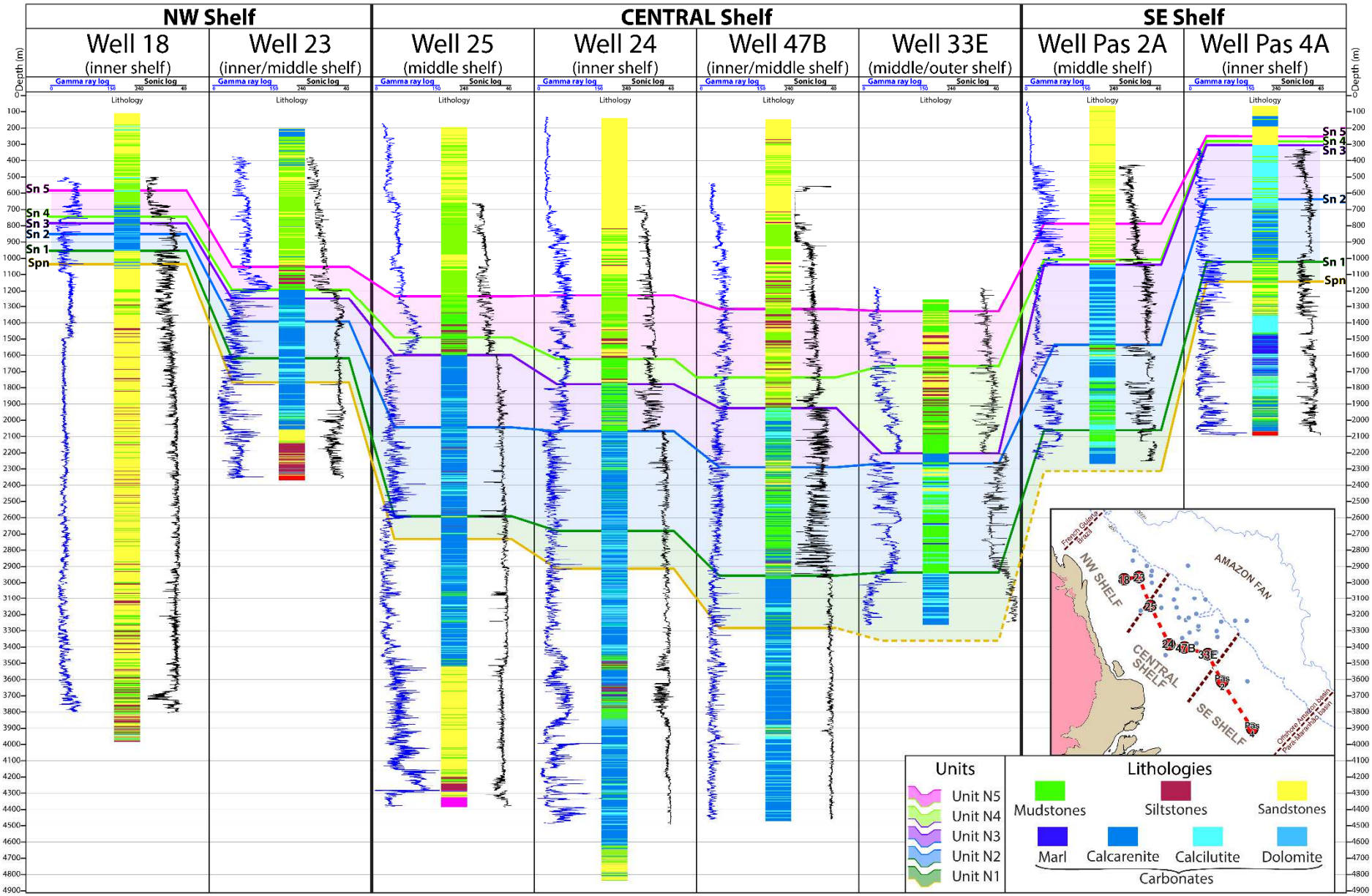

Figure 3: Regional NW-SE cross-section showing depositional unit architecture based on well control (cuttings and sidewall cores) and wireline logs (Gamma Ray and Sonic) of eight wells located in the Offshore Amazon Basin. Colored lines represent the bounding surfaces of units N1 to N5 (surfaces *Spn* and *Sn1* to *Sn5*) defined in this work. Well 33E after Figueiredo et al. (2009). Location of wells shown in Figure 1.

4.1.1. Unit N1

Unit N1 is the basal unit of the Neogene interval of the Amapá carbonates. Its lower surface *Spn* is of irregular morphology, characterized by truncation of underlying reflectors and a few incisions, pointing to an erosive nature (Figs. 4-6). Its upper surface *Sn1* varies from irregular to smooth and an erosional or depositional nature is not clear from seismic data alone. However, downlaps by the overlying unit (Figs. 4 and 6) support an interpretation of *Sn1* as a maximum flooding surface. Well reports show that unit N1 is a mixed siliciclastic-carbonate unit, the extent of carbonate-dominated strata varying across the shelf (Fig. 3).

On the NW shelf, unit N1 is mainly a relatively thin stratal package, ~130 m thick, with a tabular aggrading geometry (Fig. 4). Near the shelf-edge, unit N1 thickens to 540 m and comprises prograding clinoforms that downlap basal surface *Spn*, and completely cover underlying units across the outer shelf-upper slope area. Top surface *Sn1* is regular and smooth across the NW shelf with no evidence of erosional features. Features consistent with carbonate buildups are not observed within unit N1 across the NW shelf, within the limits of seismic resolution. However, well reports indicate that carbonate sedimentation was predominant during deposition of the unit across the mid-outer shelf, whereas siliciclastic sedimentation predominated across the inner shelf (e.g. wells 18 and 23; Fig. 3).

On the SE shelf, unit N1 mainly comprises strata with aggradational-retrogradational geometries, mostly limited to an area equivalent to the paleoshelf to upper slope of the underlying units where it is ~600 km thick, and thins considerably downslope (Fig. 5). Top surface *Sn1* is rather irregular. Internal seismic facies include aggrading mounded features across the mid-outer shelf, up to 400 m thick and 50 km wide, consistent with carbonate buildups. As in the NW shelf, lithological descriptions in well reports (e.g. wells Pas 2A and Pas 4A; Fig. 3) indicate that carbonate sedimentation was predominant across the mid-outer shelf, whereas siliciclastic sedimentation predominated on the inner shelf.

On the Central shelf, unit N1 is similar in character to the SE shelf: beneath an irregular top surface *Sn1*, it is essentially an aggradational-retrogradational unit, ~350 m thick and thinning downslope (Fig. 6). However, backstepping of the shelf-edge is seen to be caused by slide scars recording downslope sediment failure (Fig. 6). Near the outer shelf, internal reflectors locally onlap basal surface *Spn*. In contrast to the SE shelf, internal seismic facies do not include mounded features consistent with carbonate buildups. Nonetheless, well reports show that carbonate deposition took place across most of the Central shelf, and was more extensive than elsewhere in the basin during deposition of unit N1 (e.g. wells 24 and 47B; Fig. 3). Siliciclastic sediments may be locally present as trough infills (Fig. 6). We interpret the aggrading character of unit N1 to reflect widespread carbonate sedimentation across most of the Central shelf, locally disrupted by cross-cutting troughs that connected the innermost shelf to the slope (Fig. 6).

4.1.2. Unit N2

Unit N2 is bounded by basal surface *Sn1*, which varies in character as above, and by top surface *Sn2*, which is of variable but irregular morphology across the shelf, indicating an erosive nature. Well reports indicate that the lithology of unit N2 varies from predominantly carbonates to predominantly siliciclastics across the different shelf regions (Fig. 3).

On the NW shelf, N2 is essentially a tabular aggrading unit, ~150 m thick on the inner-middle shelf and thickening seaward to 460 m on the outermost shelf where it forms aggrading-prograding clinoforms (Fig. 4). On seismic profiles, across the mid to outer shelf, top surface *Sn2* includes step-like features and truncates internal clinoform reflectors. Internal seismic facies do not include features consistent with the presence of carbonate buildups (Fig. 4). However, lithological descriptions in well reports show that N2 is composed of carbonates, from the inner to outer shelf (e.g. wells 18 and 23, Fig. 3).

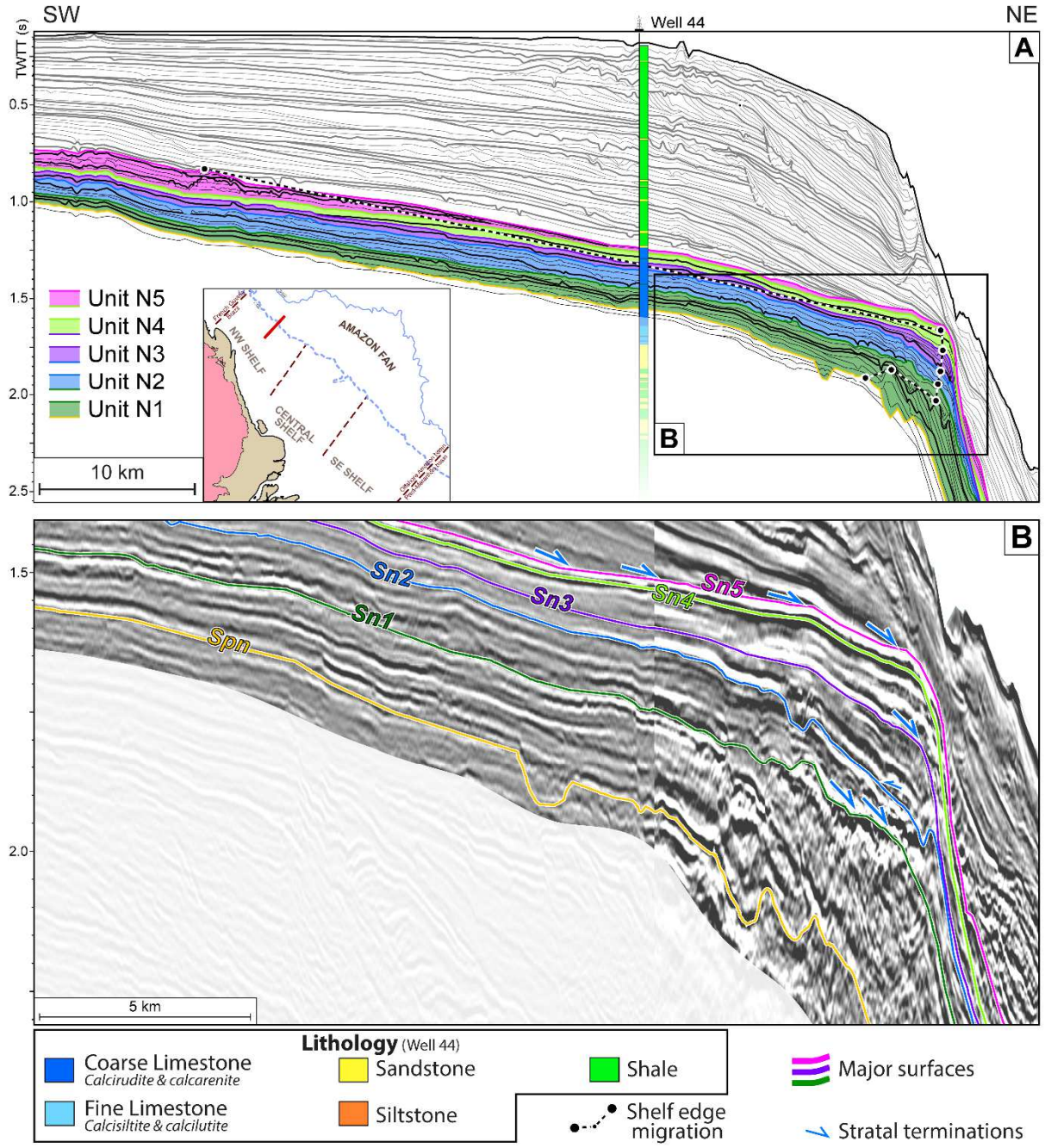

Figure 4: Interpreted seismic profile across the NW sector of the Amazon shelf (location in Figure 1) - (A) Linedrawing of the stratigraphic interpretation, highlighting the main units defined in this work; dashed line with dots indicates shelf-edge migration. (B) Detail of the outer shelf-upper slope, showing units N1 to N5 and respective bounding surfaces.

Across the SE shelf, N2 is also a mainly aggrading unit with a slight progradational character at the shelf-edge (Fig. 5). In contrast to the NW shelf, unit N2 thickens landward, from ~300 m on the outer SE shelf to up to 700 m across the inner shelf (Fig. 5).Thinning of the unit on the outer shelf may reflect greater erosion beneath top surface *Sn2* (Fig. 5).

Internal seismic facies include aggrading mounded features consistent with carbonate buildups, which vary in form and dimension across the shelf: (1) carbonate buildups up to 10 km wide in the inner shelf (Fig. 5A); (2) isolated buildups up to 3.5 km wide in the mid-shelf; and (3) flat-topped carbonate buildups up to 40 km wide in the outermost shelf (Fig. 5B). Well reports indicate that carbonate sediments dominate N2, except on the inner shelf where carbonates interfinger with siliciclastics (wells Pas 2A and Pas 4A; Fig.3).

On the Central shelf, N2 is a predominantly aggrading unit, thinner on the outer shelf (~300 m) than on the inner shelf (~600 m) and more restricted in its seaward extent than underlying unit N1 (Fig. 6). The top surface *Sn2* displays a series of steps and canyon-like incisions, reflecting intense erosion across the mid to outer shelf and upper slope (Fig. 6). Well reports show that unit N2 is composed mainly of carbonates in the western part of the Central shelf (wells 24 and 25; Fig. 3), whereas in the eastern part, in contrast to the NW and SE shelves, unit N2 is essentially composed of siliciclastics containing only thin carbonate layers (wells 47B and 33E; Fig. 3).

4.1.3. Unit N3

Unit N3 is bounded by erosive basal surface *Sn2*, and by a smooth top surface *Sn3* that presents no evidence of truncations across the shelf region (Figs. 4-6). Top surface *Sn3* corresponds to seismic surface A of Gorini et al. (2014) and Reis et al. (2016). Based on downlaps by the overlying unit (Figs 5 and 6), we interpret surface *Sn3* as a maximum flooding surface. Well reports indicate that unit N3 varies in lithology across the shelf, from carbonate-dominated to a mixed siliciclastic-carbonate composition (Fig. 3).

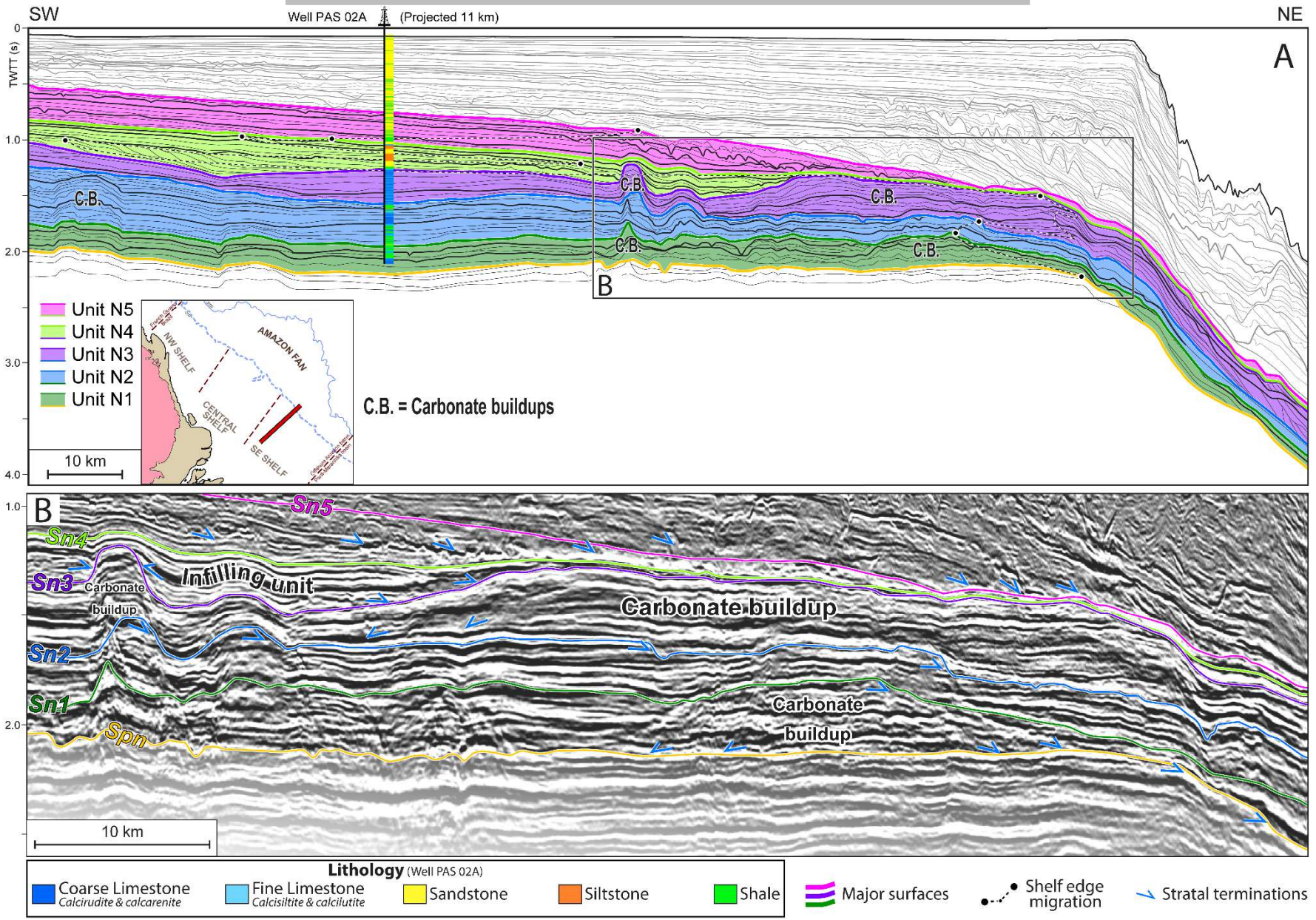

Figure 5: Interpreted seismic profile across the SE sector of the Amazon shelf (location in Figure 1) - (A) Linedrawing of the stratigraphic interpretation, highlighting the main units defined in this work; dashed line with dots indicates shelf-edge migration. (B) Detail of the outer shelf-upper slope, showing units N1 to N5 and respective bounding surfaces.

On the NW shelf, unit N3 is a tabular aggrading stratal package that is relatively thin (<160 m) and almost absent on the upper slope (Fig. 4). Near the shelf-edge, internal reflectors onlap basal surface *Sn2* (Fig. 4).Well reports show that N3 is composed of carbonates, from the inner to the outer shelf (e.g. wells 18 and 23; Fig. 3).

Across the SE shelf, N3 is an aggrading unit, thickening from ~320 m on the inner shelf to up to 550 m on the middle-outer shelf (Fig. 3). The shelf-edge within unit N3 is shifted basinwards in comparison to unit N2 in the same area (Fig. 5). Across the outer shelf, top surface *Sn3* displays steps corresponding to reflector terminations (Fig. 5), but it is not clear if these are stratal truncations due to shelf-edge erosion or apparent truncations generated by a series of retrogressive offlaps (due to backstepping of carbonate build-ups). Internal seismic facies include mounded features consistent with carbonate buildups, up to 3.5 km wide on the mid-shelf, and flat-topped carbonate buildups up to 40 km wide on the outer shelf (Fig. 5). Lithological reports indicate that the unit is predominately composted of carbonates across the shelf (wells Pas 2A and Pas 4A; Figs. 3 and 5).

On the Central shelf, N3 is an aggrading-retrograding unit up to ~360 m thick that thins basinwards (Fig. 6). Top surface *Sn3* has an irregular morphology across the outer shelf and upper slope interpreted as the expression of slide scars (Fig. 6). The shelf break reached its most proximal position during the Neogene within the upper part of unit N3 (Fig. 6). This shelf-edge retrogradation resulted in the formation of a 150-km wide embayment on the Central shelf (Fig. 7C). Irregularities in the upper part of unit N3 are mainly related to internal aggrading reflectors interpreted as carbonate buildups. Lithological data from wells 47B and 33E (Fig. 3) show that unit N3 is essentially composed of carbonates with siliciclastics limited to inner shelf positions.

4.1.4. Unit N4

Unit N4 is bounded by basal surface *Sn3* and by top surface *Sn4*, both of which are smooth. As for basal surface Sn3, downlap of *Sn4* by the overlying unit supports an interpretation as a maximum flooding surface (Figs. 5 and 6). *Sn4* is interrupted in places by deep incisions related to erosive surfaces within overlying unit N5 (Fig. 6). Well reports indicate that unit N4 is composed of carbonates on the NW shelf, but entirely of siliciclastics in the Central and SE shelf regions (Fig. 3).

Across the NW shelf, N4 is a tabular aggrading unit up to ~180 m thick, comparable to underlying unit N3 (Fig. 4). Lithological reports show that, like N3, unit N4 is composed primarily of carbonates, from the inner to the outer shelf (e.g. wells 18 and 23; Fig. 3).

Across the Central and SE shelves, seismic data analysis shows that unit N4 is essentially prograding-aggrading (Figs. 5 and 6). It is noteworthy that surface *Sn4* is the top of an infilling unit, which covers an unconformity within unit N4 above prograding clinoforms (Figs. 5 and 6). As a whole, unit N4 tends to smooth the irregular morphology of the carbonate buildups at the top of underlying unit N3 (Figs. 6 and 5). On the SE shelf, unit N4 is restricted to low areas on the inner to mid shelf which it infills (Fig. 5), whereas on the Central shelf it extends across the entire region (Fig. 6) and partially infills the large embayment previously formed in this region (Fig. 7D). Lithological data in well reports from both shelf regions show that unit N4 is purely siliciclastic in composition and overlies carbonates of unit N3 (wells 24, 47B, 33E, Pas 2A and Pas 4A; Fig. 3).

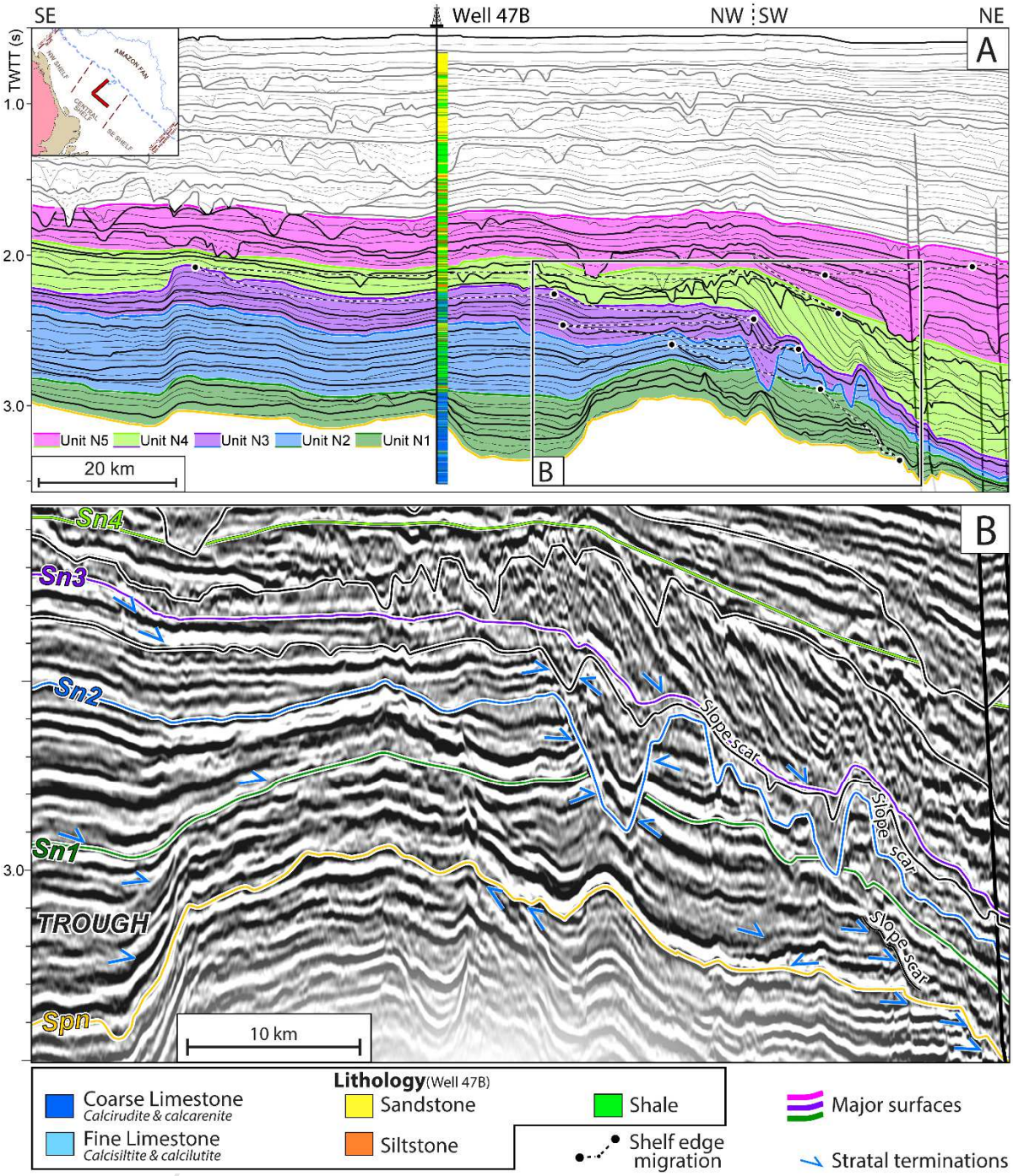

Figure 6: Interpreted seismic profile across the Central sector of the Amazon shelf (location in Figure 1) - (A) Linedrawing of the stratigraphic interpretation, highlighting the main units defined in this work; dashed line with dots indicates shelf-edge migration. (B) Detail of the outer shelf-upper slope, showing units N1 to N5 and respective bounding surfaces.

4.1.5. Unit N5

Unit N5 is bounded by smooth basal surface *Sn4* and by upper surface *Sn5*, which is also smooth. Based on downlaps by the overlying siliciclastic unit (Figs. 4 and 5), we interpret *Sn5* as a maximum flooding surface. Surface Sn5 is interrupted in places by deep incisions caused by erosion within levels of the overlying sedimentary units (Fig. 6). Well reports show that unit N5 is composed of carbonate or siliciclastic sediments (Fig. 3).

On the NW shelf, unit N5 is an aggrading package about ~150m thick across the inner to middle shelf, thinning to a tabular unit ~40m thick on the outer shelf (Fig. 4).Well reports indicate that the lower part of unit N5 is predominantly composed of carbonates, whereas its upper part is dominantly siliciclastic with thin (<10 m) carbonate layers (e.g. wells 18 and 23; Fig. 3). However, internal seismic facies include isolated mound-like carbonate buildups up to 4 km wide, most common on the inner shelf in the upper part of the unit, suggesting that isolated carbonate-dominated environments occurred sparsely distributed on the NW shelf during the final deposition of unit N5. The carbonates within the upper part of unit N5 across the NW shelf represent the last expression of the Amapá carbonates in the Offshore Amazon Basin.

On the Central and SE shelves, unit N5 consists of prograding clinoforms (Figs. 5 and 6). On the inner-middle Central shelf, the unit is about 400 m thick and thickens up to ~800 m near the shelf-edge (Fig. 6). In contrast, on the SE shelf, the unit is only up to ~230 m thick on the inner-middle shelf and thins significantly on the outermost shelf (Fig. 5).Well reports indicate that unit N5 is composed of siliciclastics in both areas (e.g. wells 47B; 33E; Pas 2A and Pas 4A; Fig. 3).

Finally, seismic data also show that across the inner to outer shelf, the thick siliciclastic units that cover unit N5 are essentially composed of seaward prograding clinoforms that downlap surface *Sn5* (Figs. 4-6), so as to completely infill the Central shelf embayment (Fig. 7E).

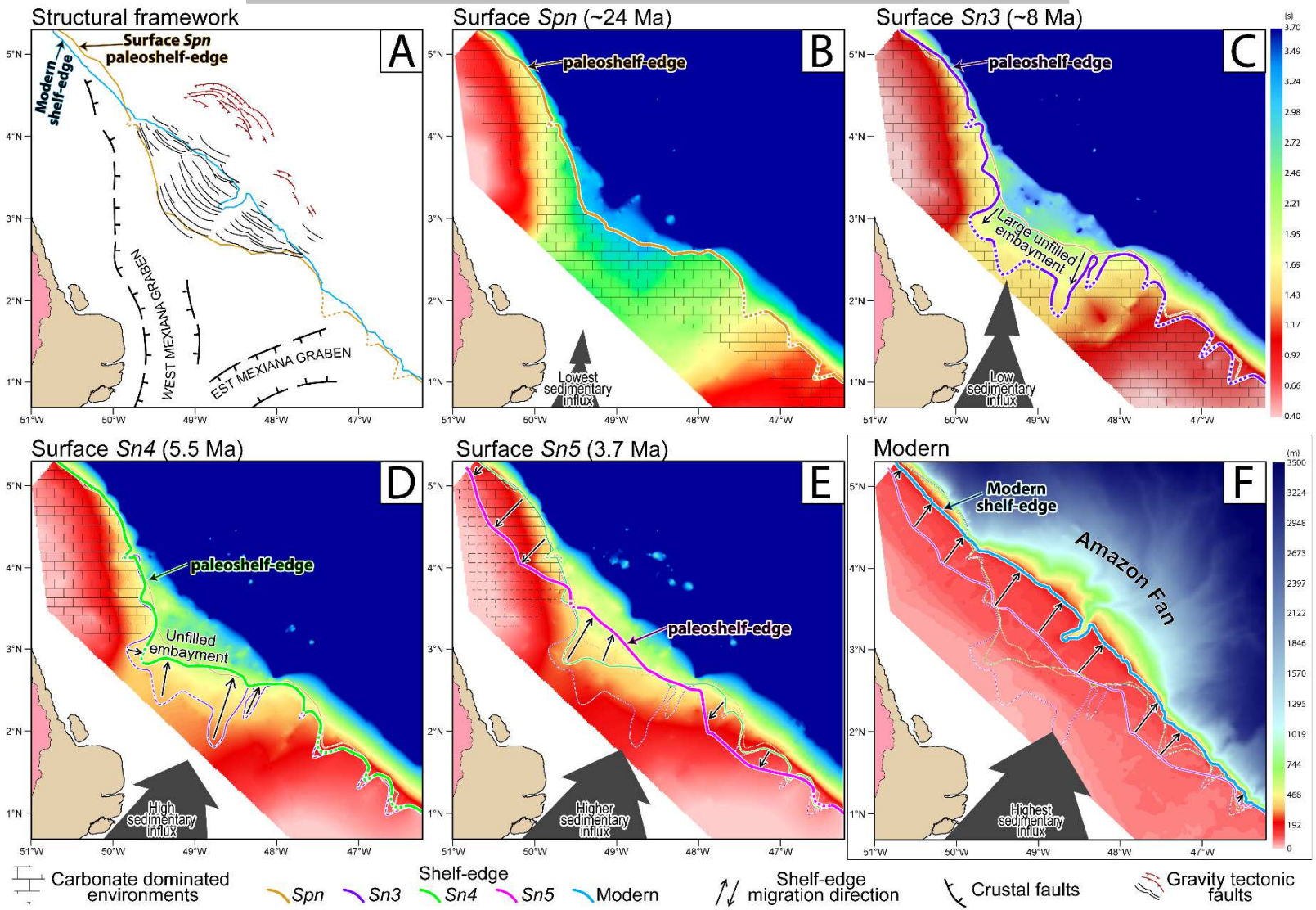

Figure 7: A - Structural framework compiled from Schaller et al. (1971) and Perovano et al. (2009). Faults associated with gravity tectonics are compiled from Perovano et al. (2009) and Reis et al. (2010). B to E - Two-way travel time (s) maps of stratigraphic surfaces mapped in this work, coupled with bathymetric maps (m) of the present-day Amazon shelf. Paleo-shelf-edge positions defined from interpreted seismic data are shown as thick colored lines. In B, note that the shelf-edge position in the central region at ca. 24 Ma was nearly coincident with the most proximal gravity tectonic-related faults. The large embayment in the Central shelf, formed due to shelf-edge retrogradation from 24 to 8 Ma, was filled between ca. 8 and 3.7 Ma, after which carbonate sedimentation on the NW shelf was finally suppressed.

4.2. *Age models of the Neogene horizons: constraining biostratigraphy by global curves of sea-level oscillations*

Age constraints for the stratigraphic surfaces bounding the five units recognized within the Neogene Amapá carbonates, (*Spn* and *Sp1-5*; Fig. 3) are based on biostratigraphic data from three exploratory wells on the Central and NW shelf (wells 33E; 45B and 47B; Figs 1, 8-10). Ages are estimated based on the position of each surface relative to the first and last occurrences of key calcareous nannofossils species in the wells, dated with reference to published chronostratigraphic compilations (Martini, 1971; Young, 1998; Raffi et al., 2006; Anthonissen and Ogg, 2012; Zeeden et al., 2013), updated to astronomically-tuned ages (Gradstein et al., 2012). Our approach of using first and last occurrences of fossil species with well-constrained ages results in a more reliable and detailed chronostratigraphic model for the Neogene succession of the Offshore Amazon Basin than those proposed in previous studies (Figueiredo et al., 2009; Cruz et al., 2014; Gorini et al., 2014). In particular, we do not rely on the predefined calcareous nannoplankton zonations applied to wells from the 1980s, based on the pioneering works of Martini (1971) and Bukry (1973), which included fossil markers used to define nannoplankton zonations that are now considered to be poorly constrained (Raffi et al., 2006). This approach was commonly used for biochronological zonation at the time most wells in the Offshore Amazon Basin were drilled, and a simple recalibration of these pre-defined zones to modern time scales could lead to substantial imprecision. Where appropriate, we also make use of other calcareous nannoplankton fossils that have been found to be useful in terms of chronostratigraphy in recent works (see Raffi et al., 2006 and Zeeden et al., 2013).

Biostratigraphic data revised as described above were subsequently correlated to global curves of sea-level oscillations (Fig. 11), to allow to better constrain ages of the Neogene stratigraphic surfaces, and thus of the deposition of units N1 to N5.

4.2.1. ***Surface Spn*** *(unit N1 basal boundary)*

In well 45B (Fig. 10), surface *Spn* corresponds to the last recorded occurrence of *Reticulofenestra bisecta* and *Cyclicargolithus abisectus* (23.13 to 24.67 Ma; Anthonissen and Ogg, 2012). In well 47B (Fig. 8), the same surface lies ~150 m below the first recorded occurrence of *Helicosphaera carteri* (22.03 Ma; Anthonissen and Ogg, 2012). These fossil markers constrain the age of surface *Spn* to between 24.67 Ma (in well 45B) and 22.03 Ma (in well 47B).

Surface *Spn* has an erosional character (Figs. 4-6), and comparison of its age range (22.03 to 24.67 Ma) to global sea-level curves (Fig. 11) shows it to encompass a pronounced sea-level fall at ca. 24 Ma in the curves of both Haq et al. (1987) and Miller et al. (2005). We propose an age of latest Oligocene to earliest Miocene (ca. 24 Ma) for this erosive surface (Fig. 6), marking it as the approximate base of the Neogene sedimentary succession in the Offshore Amazon Basin.

4.2.2. **Surface *Sn1*** (top of unit N1, base of unit N2)

In well 47B (Fig. 8), surface *Sn1* corresponds to the last recorded occurrence of *Sphenolithus belemnos* (17.95 to 19.03 Ma; Anthonissen and Ogg, 2012) and lies only ~15 m below the first recorded occurrence of *Sphenolithus heteromorphus* (17.71 Ma; Anthonissen and Ogg, 2012). These fossil markers in well 47B constrain the age of Surface *Sn1* to between 17.71 and 19.03 Ma.

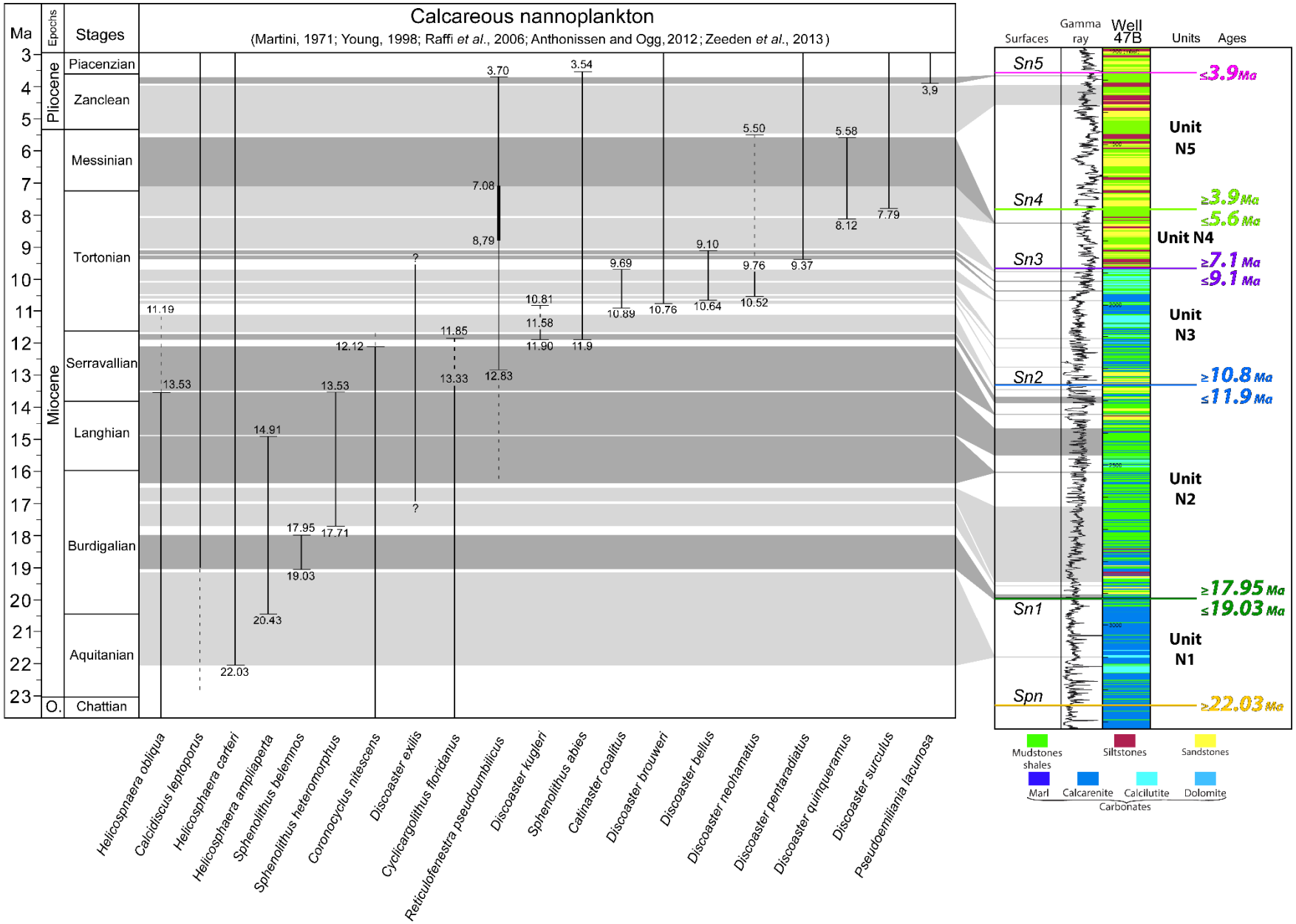

Figure 8: Chronostratigraphic model for well 47B on the Central Shelf (location in Figure 1). Ages are based on the first and last occurrences of the indicated calcareous nannofossil species.

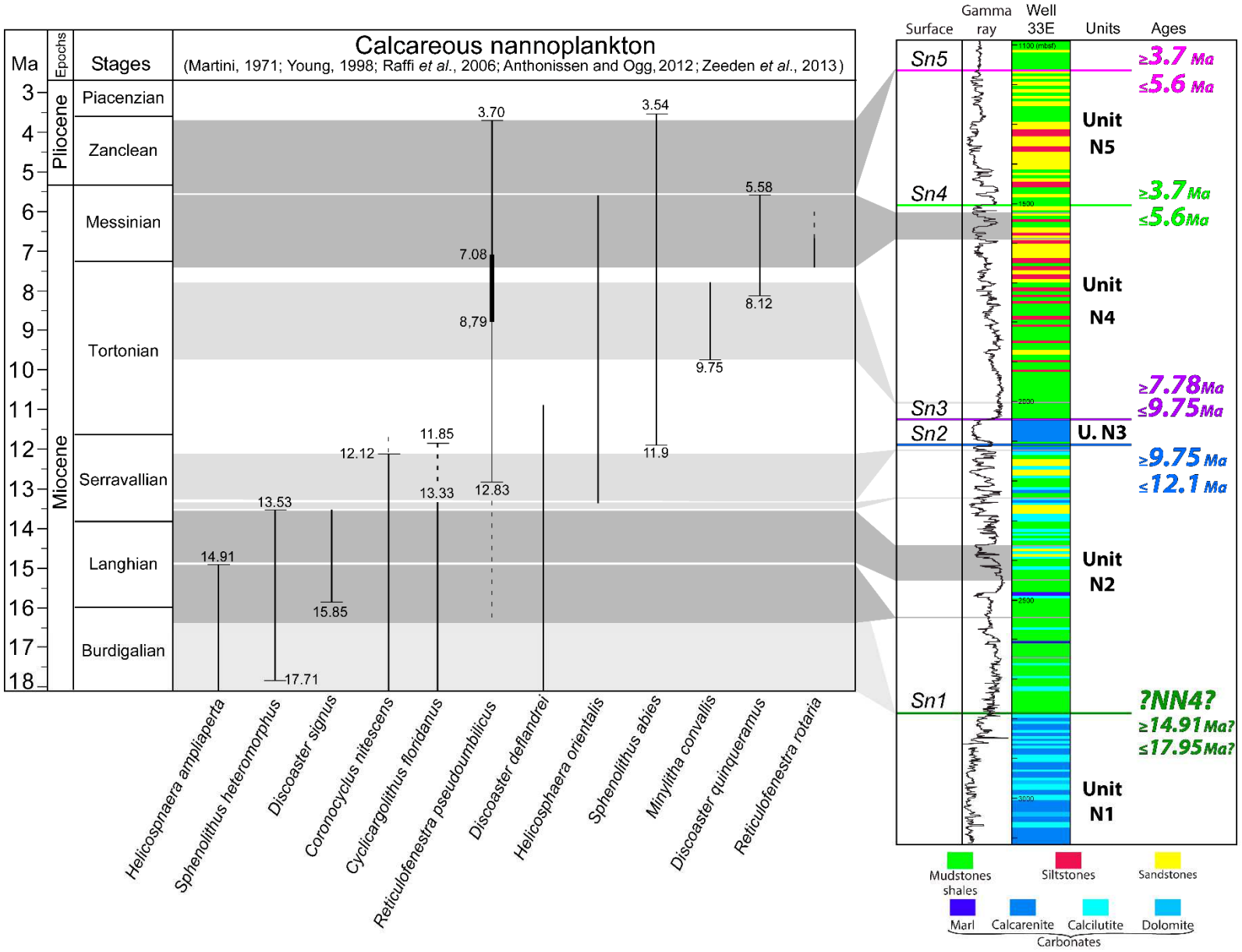

Figure 9:Chronostratigraphic model for well APS 33E on the Central Shelf (location in Figure 1). Ages are based on the first and last occurrences of the indicated calcareous nannofossil species.

Surface *Sn1* has a smooth non-erosive character, and comparison of its biostratigraphic age range (17.71 to 19.03 Ma) to global sea-level curves shows that it spans the inflexion point of a major Burdigalian global sea-level rise (Fig. 11). We interpret surface *Sn1* as a maximum flooding surface at ca. 18 Ma (Fig. 11). This suggests that the mid-outer shelf aggrading mounds of seismic unit N1 are carbonate buildups formed in the context of transgressive and highstand depositional systems.

4.2.3. **Surface *Sn2*** (top of unit N2, base of unit N3)

In well 47B, the occurrence range of *Discoaster kugleri* (10.8 to11.93 Ma; Zeeden et al., 2013) begins ~40 m below surface *Sn2* and ends ~55 m above it (Fig. 8). Thus, the age of surface *Sn2* lies between 10.8 and 11.93 Ma.

Surface *Sn2* is an erosional unconformity, including evidence of deeply-incised channel-like features (Fig. 6). Comparison to global sea-level curves allows us to correlate *Sn2* with the major Tortonian sea-level fall, whose maximum fall, and final erosion, is dated at ca. 11 Ma (Haq et al., 1987; Miller et al., 2005).

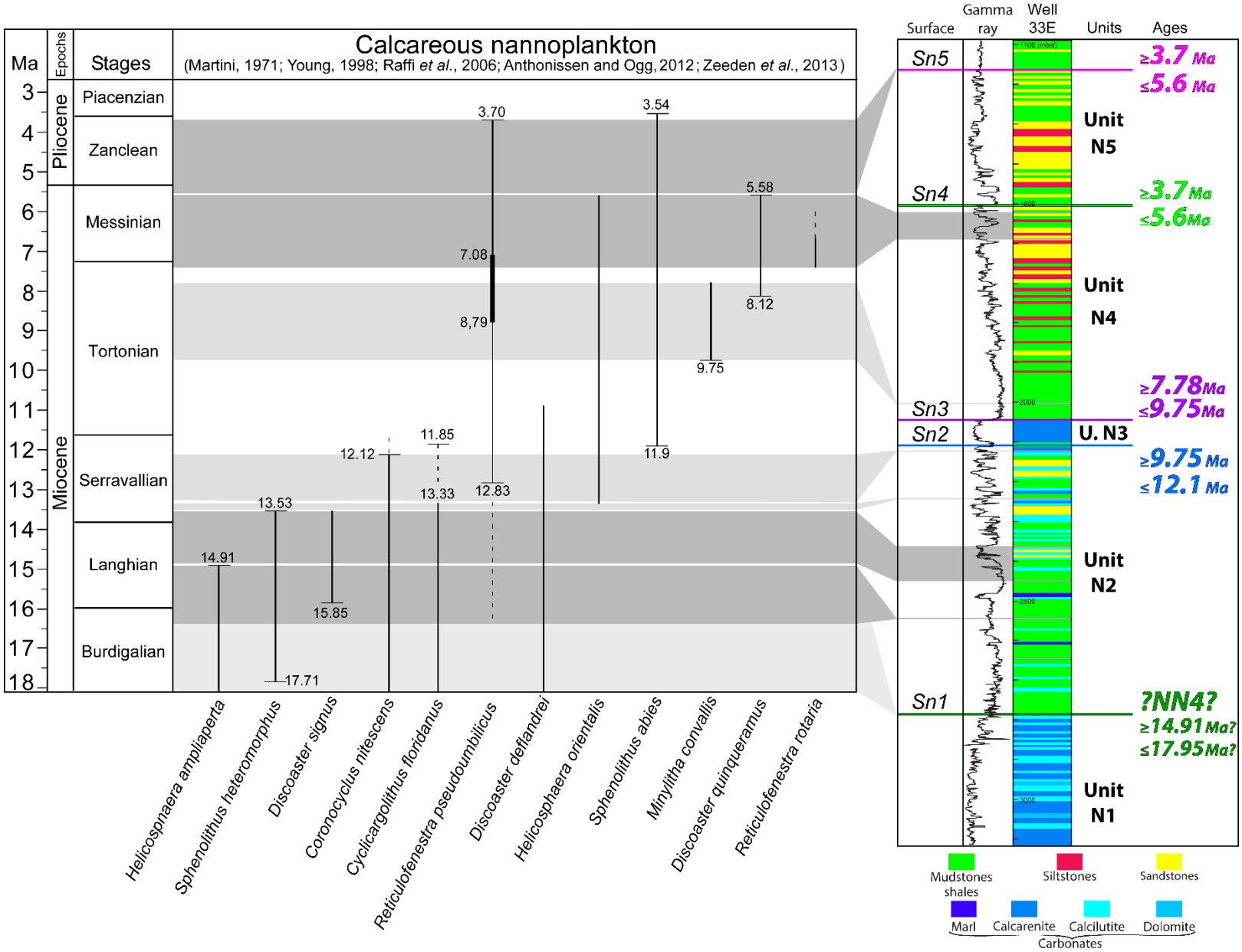

Figure 10: Chronostratigraphic model for well 45B on the NW Shelf (location in Figure 1). Ages are based on the first and last occurrences of the indicated calcareous nannofossil species.

4.2.4. **Surface *Sn3*** (top of unit N3, base of unit N4)

Surface *Sn3* corresponds to the top of the Amapá carbonates in the Central shelf (Fig. 6). In well 47B, *Sn3* lies ~30 m above the first coherent occurrence of *Discoaster quinqueramus* (dated at 8.12 Ma in the North Pacific, Anthonissen and Ogg, 2012) and ~40 m above the highest recorded occurrence of *Discoaster bellus* (dated at 9.1 Ma in the Equatorial Atlantic; Zeeden et al., 2013). Also in well 47B, surface *Sn3* is equivalent to the highest sampled level within the *Reticulofenestra pseudoumbilicus* paracme (8.794 to 7.087 Ma; Zeeden et al., 2013). In well 33E, surface *Sn3* is overlain by sediments containing *Minylitha convallis* (Fig. 9), whose last consistent occurrence in the Equatorial Pacific took place between 8.3 and 7.78 Ma (Raffi et al., 2006). Assuming similar ages in the Atlantic Ocean for the last occurrence of *Minylitha convallis* and the first occurrence of *Discoaster quinqueramus*, the age of surface *Sn3* lies between 7.78 and 8.12 Ma. More conservatively, considering that precise ages for the last occurrence of *Minylitha convallis* and the first occurrence of *Discoaster quinqueramus* in the Equatorial Atlantic remain to be verified, the age of surface *Sn3* must lie between 7.087 and 9.1 Ma.

Surface *Sn3* has a smooth, non-erosive seismic character and is downlapped by overlying strata on the inner shelf (Figs. 5 and 6), In the time span of 7.087 to 9.1 Ma, global sea-level curves from Haq et al. (1987) and Miller et al. (2005) show an inflexion point of a transgressive sea-level trend at ca. 8 Ma (Fig. 11). We interpret *Sn3* as a maximum flooding surface, formed during the global highstand at ca. 8 Ma. In this context, internal features identified across the SE and Central shelves of the Offshore Amazon Basin during deposition of unit N3 are interpreted as carbonate buildups of varying width, formed as a response to the sea-level rise and shoreline transgression prior to ca. 8 Ma.

4.2.5. **Surface *Sn4*** (top of unit N4, base of unit N5)

In well 47B (Fig. 8), surface *Sn4* lies ~50 m above the last recorded occurrence of *Discoaster quinqueramus* (precisely dated at 5.58 Ma; Anthonissen and Ogg, 2012), while in well 45B (Fig. 10) it lies ~100 m below the first recorded occurrence of *Discoaster tamalis* (4.1 Ma; recalibrated after Young, 1998). These fossil markers indicate the age of surface *Sn 3* to lie between 5.58 and 4.1 Ma.

Within the time span of 5.58 to 4.1 Ma, *Sn4* can be correlated to an inflexion point of a sea-level rise at ca. 5.5 Ma on curves from both Haq et al. (1987) and Miller et al. (2005) (Fig.11). We interpret *Sn4* as a maximum flooding surface, consistent with seismic evidence of a smooth non-erosive character and downlaps by the overlying unit (Figs. 4 and 5).

4.2.6. **Surface *Sn5*** (top of unit N5)

In well 45B, surface *Sn5* lies ~40 m above the top of the occurrence of the Amapá carbonates, at the stratigraphic level of the last recorded occurrence of *Reticulofenestra pseudoumbilicus* (Fig. 10), which indicates an age no younger than 3.7 Ma for this surface (Anthonissen and Ogg, 2012). In well 47B (Fig. 8), *Sn5* lies only ~10 m above the highest sampled level containing *Reticulofenestra pseudoumbilicus* and *Pseudoemiliania lacunosa* (at least as old as 3.9 Ma; recalibrated after Young 1998). These fossil markers constrain surface *Sn5* to an age between 3.9 and 3.7 Ma.

Comparison to global sea-level curves shows that this surface can be correlated to a sea-level rise close to the Zanclean/Piacenzian boundary, dated at ca. 3.7 Ma considering the curves of both Haq et al. (1987) and Miller et al. (2005) (Fig. 11). We interpret *Sn5* as a maximum flooding surface, consistent with seismic evidence of a smooth non-erosive character and downlaps by the overlying unit (Figs. 4-6).

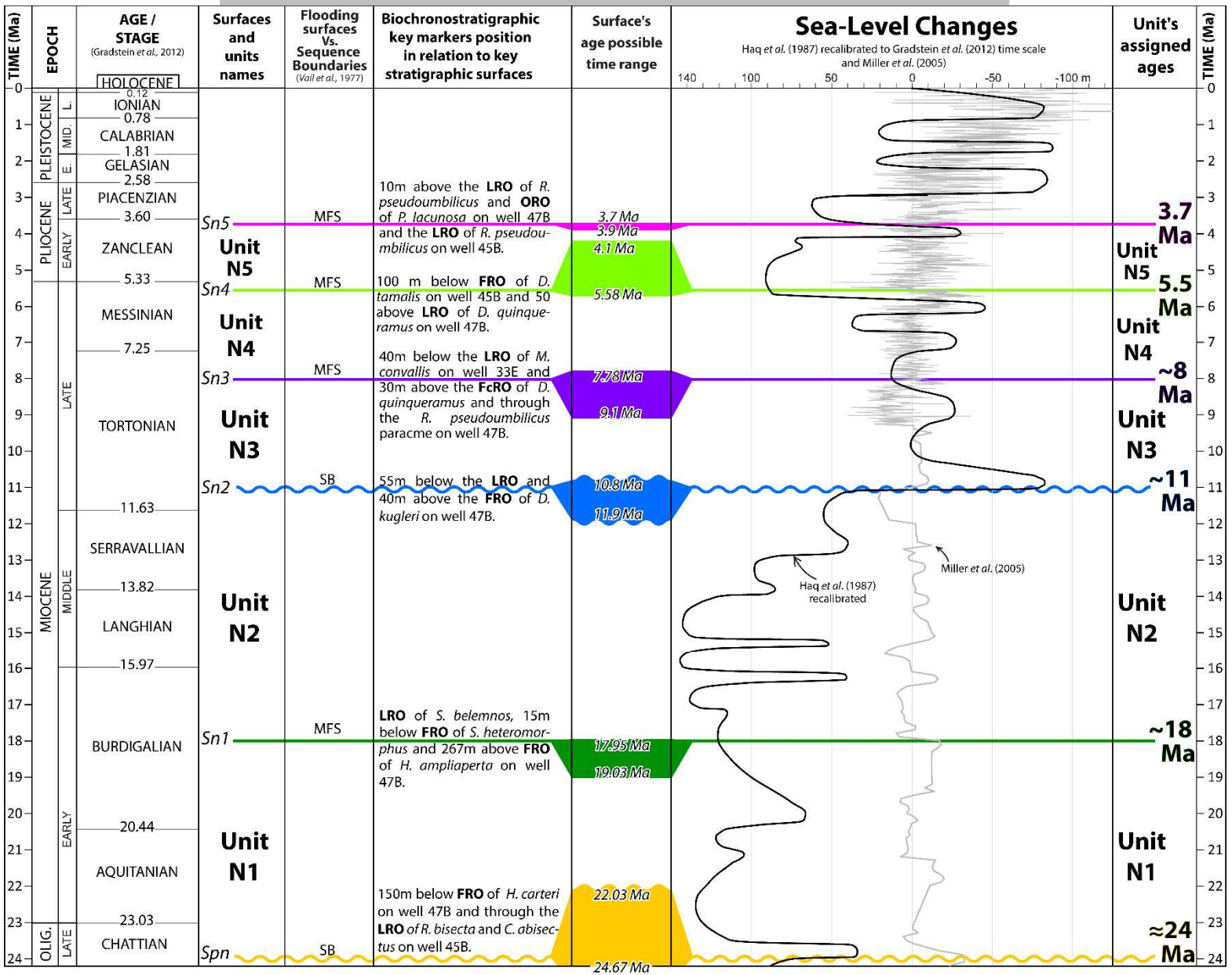

Figure 11: Chart summarizing the proposed age model for sequences N1 to N5 and their correlation to geological ages of Gradstein et al. (2012). Unit ages are based on biostratigraphic data from the wells in Figures 8-10, refined by correlation with the global sea-level curves of Haq et al. (1987) and Miller et al. (2005).

4.3. Calculation of non-eustatic accommodation space

The creation of non-eustatic accommodation space across the Offshore Amazon Basin during deposition of the upper Amapá carbonates was estimated using the measured thickness and proposed ages of units N1 to N5 in seven wells across the inner-middle shelf (Fig. 12). These wells are all in positions where seismic interpretation indicates that there was no significant erosion during deposition of units N1 to N5.

Non-eustatic accommodation space was calculated for each unit by subtracting from undecompacted unit thicknesses the maximum eustatic sea level rise during the corresponding time interval, considering curves from both Haq et al. (1987) and Miller et al. (2005). The results represent a minimum estimate of the amount of accommodation space required at each well location during the deposition of units N1 to N5, in order to allow deposition of their measured thicknesses

Considering the shelf as a whole, several overall trends are apparent for the Neogene sedimentary succession of the Offshore Amazon Basin:

i. Rates of non-eustatic accommodation space increased from ca. 18 to 8 Ma, decreased during a more quiescent phase between 8 and 5.5 Ma, and subsequently increased again to reach a maximum during the Quaternary (Fig. 12);
ii. Comparing the different shelf regions, rates were consistently higher on the Central shelf since 24 Ma, resulting in a greater depth of paleosurfaces there (Fig. 7);
iii. Rates of creation of non-eustatic accommodation space varied between the NW and SE shelves prior to and after 8 Ma; before this time, rates were higher on the SE shelf, while after 8 Ma they were higher on the NW shelf. This can be seen by comparing wells at similar positions on the SE and NW shelves, e.g. inner shelf wells 23 and Pas 4A, or mid-shelf wells 18 and Pas 2A (Fig. 12).

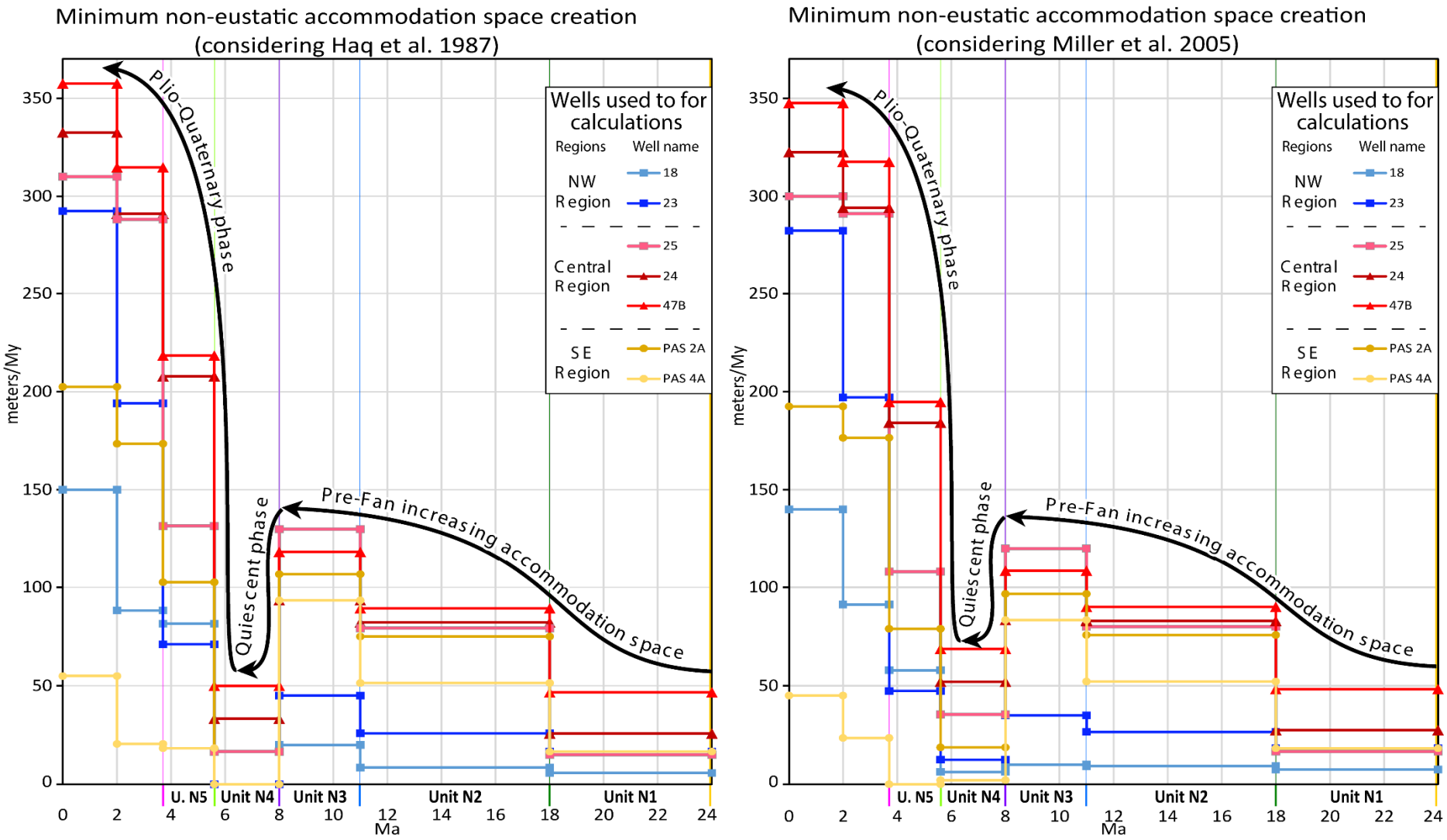

Figure 12: Graphs summarizing estimates of the non-eustatic accommodation space required for the deposition of each Neogene sedimentary unit on the Amazon shelf, based on subtracting the maximum eustatic rise during the corresponding time interval (at left from Haq et al. 1987, at right from Miller et al. 2005) from the undecompacted thicknesses of units N1 to N5.

5. DISCUSSION

The results above provide a new picture of the Neogene stratigraphic and paleo-geographical evolution of the Offshore Amazon Basin, including a more detailed characterization of changes in carbonate and siliciclastic deposition across the continental shelf. In this section, we first examine the deposition of the Neogene units in relation to variable rates of creation of non-eustatic accommodation space along the shelf, the patterns of which we argue to indicate differential subsidence in response to tectonism and/or loading. We then discuss the spatial and temporal evolution of the Amazon shelf, recognizing four main Neogene stages that are discussed in relation to possible controlling factors on carbonate vs siliciclastic depositional environments.

5.1. *Non-eustatic accommodation*

Accommodation space creation in marine environments is argued to be mainly controlled by the interaction of eustatic variations with sediment supply and subsidence (Catuneanu, 2002). Subsidence includes the effects of isostatic compensation for loading by sediment and water, as well as the underlying tectonic subsidence (which may be due to rifting, cooling and flexure). By subtracting the eustatic component from the undecompacted thickness of stratigraphic units (subsection 4.3), we obtain a minimum estimate of the accommodation space created by all forms of subsidence (Fig. 12). Our approach accounts for estimates of a minimum amount of non-eustatic accommodation that must have been created in the time spam of each sedimentary unit, in order to enable the deposition of the measured thickness of units N1 to N5.

This approach underestimates accommodation space creation in three main aspects: (i) decompacted sedimentary units would result in larger values, while differential compaction of differing lithologies implies spatially variable changes in the thickness of each unit that are unresolved; (ii) using a maximum value for eustasy assumes that all accommodation space created by sea-level rise would be immediately filled. This is unlikely for short-lived eustatic changes that occurred during deposition of units N1 to N5 (e.g., the Zanclean sea-level rises reported by Miller et al., 2005; Fig. 11); (iii) we have also to consider that erosion may have thinned the measured thickness of sedimentary units.

All these issues are mitigated on the Amazon shelf by the fact that, on the inner-middle shelf, short-lived eustatic rises should account for no more than a few tens of meters of uncertainty, versus sedimentary unit thicknesses of hundreds of meters; and the same is true for differential compaction. Uncertainties in the sea-level curves seem to be of secondary importance as the overall trends of calculated minimum non-eustatic accommodation are the same (Fig. 12) in scenarios considering sea-level curves of both Haq et al. (1987) and Miller et al. (2005). This fact indicates that non-eustatic factors are the most relevant in the long-term accommodation space creation in the Amazon shelf. Furthermore, seismic analysis was used to choose wells located in regions were no significant erosion was observed neither on the base nor on the top of each sedimentary unit.

In this context, the rates of non-eustatic accommodation space presented in Figure 12 provide qualitative information on Neogene variations in subsidence across the shelf. The trends in Figure 12 indicate that since at least 24 Ma, the Offshore Amazon Basin was affected by increasing rates of non-eustatic accommodation space creation that varied across the three shelf sectors (NW, Central and SE), resulting in greater thicknesses of units N1-N5 on the Central shelf (Figs. 3-6). This indicates that the margin was affected by greater subsidence in the Central shelf, which could be due to localized extension and/or cooling, or

along-shelf flexure of the lithosphere. There is no seismic evidence of extension during the deposition of the units, and the thermal effects of Triassic-Jurassic rifting should be minimal in the Neogene (Allen and Allen, 2005). However, the varying crustal structure of the Amazon shelf (a series of deeply-buried extensional structures beneath the Central shelf) inherited from the Atlantic Rift (Fig. 7A; Schaller et al., 1971) could have influenced along-shelf differential flexure.

Intense flexural subsidence of the Offshore Amazon Basin has been classically attributed to a loading effect of rapid deposition of the Amazon fan (e.g. Driscoll and Karner, 1994). However, our estimates of non-eustatic accommodation space show that the differential subsidence of the Amazon shelf since 24 Ma long pre-dates the initiation of the Amazon fan, recently dated by Hoorn et al (2017) to between 9.4 and 9 Ma. We suggest instead that greater subsidence in the Central shelf was responsible for capturing sediment input, thus acting as a major control on the distribution of depocenters, and accounting for their location more than 200 km northward of the Amazon River mouth. In this interpretation, flexural subsidence caused by loading of the Amazon fan acted as a positive feedback on a margin that was already prone to differential subsidence prior to the onset of higher sediment influx after 9 Ma. Along-shelf differential subsidence may also explain why, during the deposition of units N2 to N3 (18 to 8 Ma), carbonate-dominated environments could be persistent and distributed across the more quiescent NW shelf, whereas on the Central and SE shelves the carbonate factory was only intermittently active due to higher rates of accommodation creation that favored the drowning of carbonate-secreting organisms.

Burial of the Amapá carbonate platform has been associated with a late Miocene onset of the transcontinental Amazon River (Figueiredo et al., 2007; Figueiredo et al., 2009). Alternatively, onshore evidence may indicate that a transcontinental Amazon River formed only later in the Pliocene (Latrubesse et al., 2010). Considering the latter possibility, we

propose that the short-lived reduction of accommodation space creation at around 8 Ma (Fig. 12) provides an alternative explanation for the suppression of carbonate production on the Central and SE Amazon shelves. In a scenario of reduced accommodation space creation at around 8 Ma, sediment would no longer be "held" on the coastal-innermost shelf region as happened between 24 and 8 Ma, allowing proximal siliciclastic systems to advance over the Central and SE shelves and suppress carbonate production. This model allows us to explain the suppression of carbonate deposition on the Amazon margin without assuming an enlargement of the paleo-Amazon River catchment area as previously proposed (e.g. Castro et al., 1978; Silva et al., 1999; Dobson et al., 2001; Figueiredo et al., 2007; Figueiredo et al., 2009; Hoorn et al., 2017). Nevertheless, this hypothesis and that of the onset of a late Miocene transcontinental Amazon River are not mutually exclusive.

5.2. Spatial and temporal evolution of carbonate- vs siliciclastic-dominated environments

Our results on the stratal architecture and age of the Amazon mixed carbonate-siliciclastic shelf allow us to divide its Neogene history into four main depositional stages: 1) from ca. 24 to 8 Ma the Amazon shelf was characterized by a predominantly aggrading mixed carbonate-siliciclastic shelf; 2) from ca. 8 to 5.5 Ma the Amazon shelf was subjected to increasing volumes of siliciclastic input, with different implications for carbonate deposition in the NW, Central and SE shelf sectors; 3) from 5.5 to 3.7 Ma the Central shelf embayment became gradually filled by sediments from the paleo-Amazon River, resulting in the progressive burial of carbonates in the NW shelf; and 4) from 3.7 Ma to present the Amazon shelf became essentially siliciclastic. Below we consider these depositional stages in

relation to possible controls by sea-level change and along-shelf variations in accommodation space creation.

Stage 1 (from ca. 24 to 8 Ma)

We argue that the predominantly aggrading trend of a mixed carbonate-siliciclastic shelf that prevailed in the basin during the deposition of N1-N3 was caused by a combination of global sea-level rise during the deposition of unit N1 (between ca. 24 and 18 Ma; Haq et al., 1987; Fig.11) and the subsequent increase in rates of creation of non-eustatic accommodation space during deposition of units N2 to N3.

During deposition of unit N1, the Amazon shelf experienced laterally variable trends of shelf-edge migration: the SE and Central Amazon shelves underwent a general landward migration of the shelf break (together with carbonate backstepping and upper slope sedimentary collapse), while progradation was observed on the NW shelf (Figs. 4 to 7).These contrasting trends of sedimentary architecture in different shelf sectors were most likely a result of along-shelf differential subsidence. As shown above (section 4.3), between ca. 24 and 18 Ma rates of creation of non-eustatic accommodation space were comparatively low on the Amazon shelf, although higher on the SE and Central shelves than in the NW shelf. An additional factor controlling shelf-edge migration may have been better conditions of carbonate production on the NW shelf, which is located farther from the proto-Amazon River - the main source of terrigenous sediment input. The NW shelf seems to have evolved in an architectural trend similar to that of a pure carbonate shelf, which exports higher volumes of sediments (reworked carbonates) toward the slope region during highstands and is less prone to drowning during eustatic rises (e.g., Handford and Loucks, 1993; Schlager et al., 1994; Betzler et al., 2013). In this context, with comparatively higher terrigenous influx, the Central and SE regions behaved in a manner similar to that of a typical siliciclastic platform, which tends to retrograde during significant rises in sea level (Catuneanu, 2002).

Differential subsidence appears to have affected carbonate production on the Amazon shelf after about 18 Ma. At that time, the carbonate platform on the Central shelf was drowned, most likely due to greater accommodation space creation (Fig. 12) combined with global sea-level rise (Haq et al., 1987; Miller et al., 2005; Fig. 11) and carbonate sedimentation was replaced by predominantly siliciclastic sedimentation (Fig. 13). An additional restraining factor for carbonate production on the Central shelf during Stage 1 may have been a comparatively higher influx of terrigenous sediments (mostly muddy), capable of reducing the availability of hard substrate and of increasing the turbidity in the water column, both of which are critical parameters for carbonate-secreting organisms (Woolfe and Larcombe, 1998). In any case, prior to ca. 18 Ma, terrigenous sedimentation never prevailed over carbonate production on the Central shelf, being restricted to troughs that conducted siliciclastic sediments directly to the slope (Fig. 13). Meanwhile, on the SE and NW shelves, where rates of accommodation space creation were lower (Fig. 12), carbonate production was able to persist throughout the middle-outer shelf domains, while siliciclastic proximal systems retreated progressively landward (Marajó Formation) to persist only on the inner shelf (Figs. 14 and 15).

During deposition of unit N2, between ca. 18 and 11 Ma, along-shelf variations in accommodation space creation were also a major controlling factor on sedimentary architecture along the Amazon shelf. During this period, the creation of non-eustatic accommodation space increased notably on the SE and Central shelves (Fig. 12), but differences in stratal architectures and carbonate distribution indicate that subsidence acted differently over these two shelf sectors. A contrasting trend of shelf-edge migration across different sectors of the Amazon shelf persisted, as the edge of the Central shelf continued to retrograde and the NW shelf prograded, while the SE shelf-edge also experienced a slightly prograding trend. It is likely that a prolonged sea-level fall between ca. 15 and 11 Ma

(Langhian-Serravalian; Haq et al., 1987; Fig. 11) favored progradation of the SE shelf during deposition of unit N2, given high rates of non-eustatic accommodation space during this period (Fig. 12). Meanwhile, on the Central shelf, high rates of accommodation space creation may have compensated a trend of falling sea level until the end of the deposition of unit N2, when the dramatic early Tortonian sea-level lowstand (Haq et al., 1987; Miller et al., 2005; Fig. 11) led to exposure of the entire shelf. Deep and large incisions observed the in seismic profiles (Fig. 6B) are evidence of erosion by rivers and large-scale slope instabilities.

A dramatic eustatic drop that occurred at the beginning of the late Miocene (ca. 11 Ma; Haq et al., 1987; Miller et al., 2005; Fig. 11) resulted in deep incisions and extensive surface truncations across the Central shelf (Figs. 6 and 13). According to Haq et al. (1987), after this major sea-level drop, global sea level rose during the late Miocene, but remained lower than in the early-middle Miocene (Fig. 11). We therefore suggest that the reestablishment of carbonate production on the Central shelf during the deposition of unit N3 (ca. 11 to 8 Ma) was a consequence of the extended eustatic lowering in the late Miocene, which may have partially compensated the intense creation of non-eustatic accommodation space in the region. During the deposition of unit N3, the same eustatic lowering enabled carbonate-secreting organisms to colonize more distal portions of the SE shelf (Fig. 14).

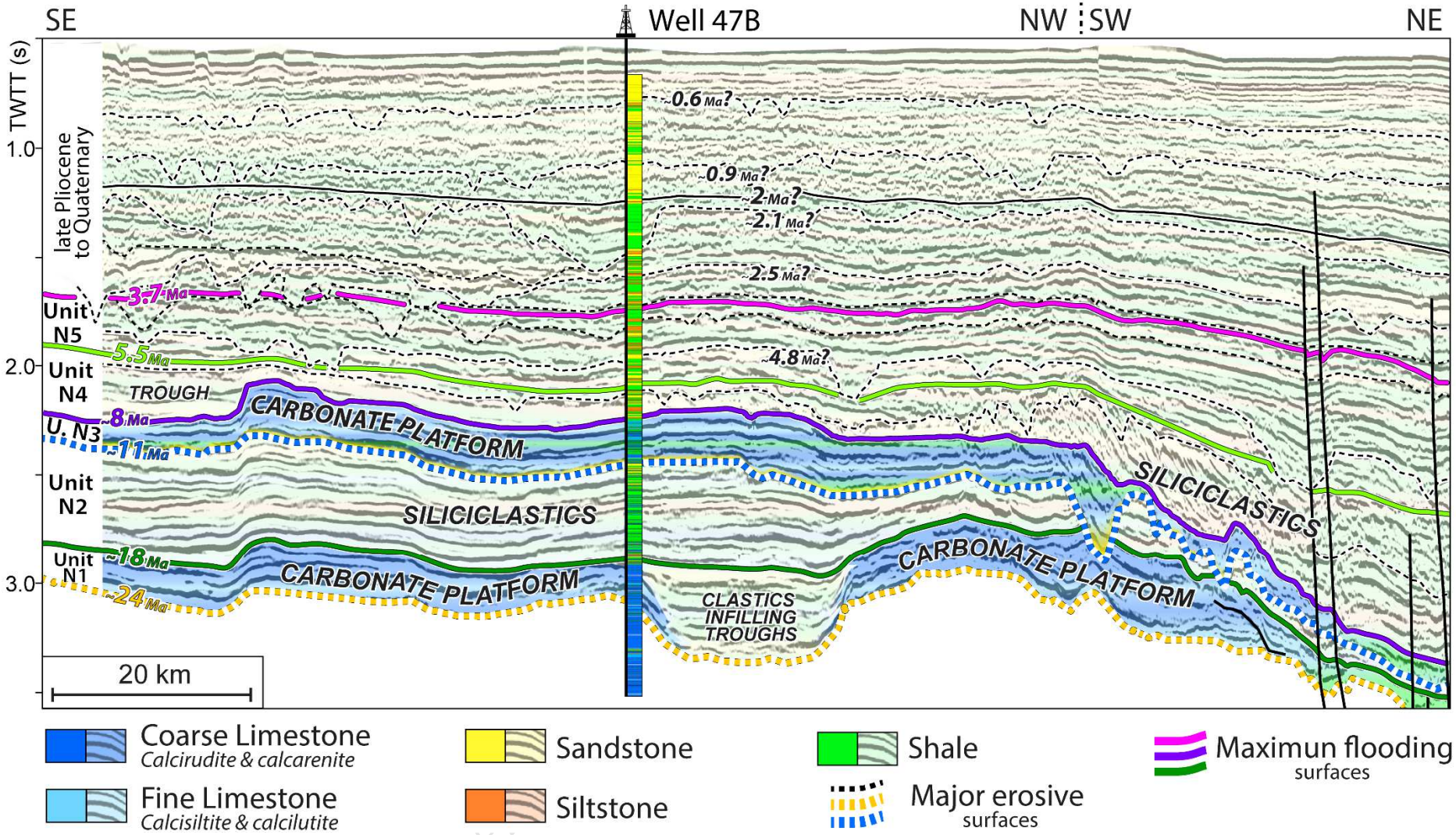

Figure 13: Interpreted seismic profile (location in Figure 1) highlighting each age-constrained surface across the Amazon shelf, together with lithological interpretations based on correlation to well 47B (and neighboring wells). Note that carbonate sedimentation resumed above the Tortonian erosive surface (ca. 11 Ma, blue dashed line) and persisted until ca. 8 Ma when a prograding siliciclastic wedge covered the shelf. Pliocene-Quaternary sequence boundaries (black dashed lines) after Gorini et al. (2014).

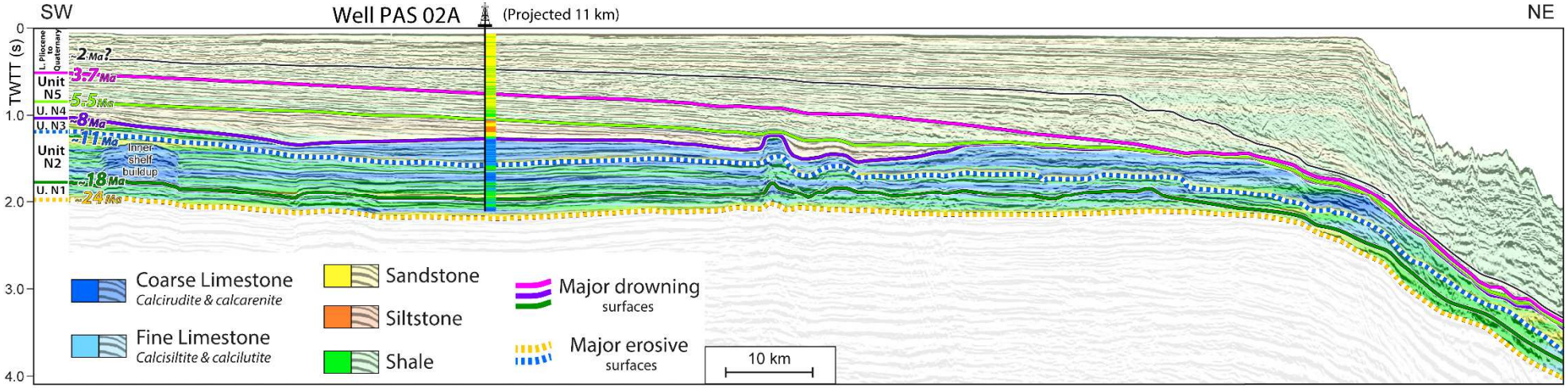

Figure 14: Interpreted seismic profile (location in Figure 1) highlighting each age-constrained surface across the Amazon shelf, together with lithological interpretations based on correlation to well Pas 02A (and neighboring wells). Note that carbonate sedimentation resumed above the Tortonian erosive surface (ca. 11 Ma) in the form of carbonate buildups.

For both the Central and SE shelves, lithological data also reveal that unit N3 records the last expression of the Amapá carbonates in these regions (Figs. 3, 5 and 6). At around 8 Ma, the Amazon shelf experienced its most important environmental change during the Neogene, as terrigenous sediments began to be supplied in volumes large enough to bury the carbonate units of the Central and SE shelves. Correlation of seismic profiles and our age model to global sea-level curves indicates that the cessation of carbonate production on the Central and SE shelves was coeval with a sea-level highstand during the latest Tortonian (Fig. 11), as previously proposed by Carozzi (1981). In this context, it is interesting to note that the death of the carbonate platform in the Central and SE shelves probably post-dates the onset of deposition of the Amazon fan, rather than pre-dating it as reported by Hoorn et al. (2017). According to these authors, high sedimentary fluxes marked the beginning of fan deposition between 9.4 and 9 Ma, whereas our biostratigraphic data point to a cessation of carbonate production on the Central and SE shelves later on, at some point between 7.78 and 9.1 Ma (most likely around 8 Ma; Figs. 13 and 14). However, as our age model shows that the oldest possible age for the top of the Amapá carbonates in the Central and SE shelves (9.1 Ma) is comparable to the earliest possible age for the Amazon fan initiation (9 Ma), the two events may have been coeval. Nonetheless, long-lasting carbonate production most likely persisted on the shelf after the onset of deposition of the Amazon fan.

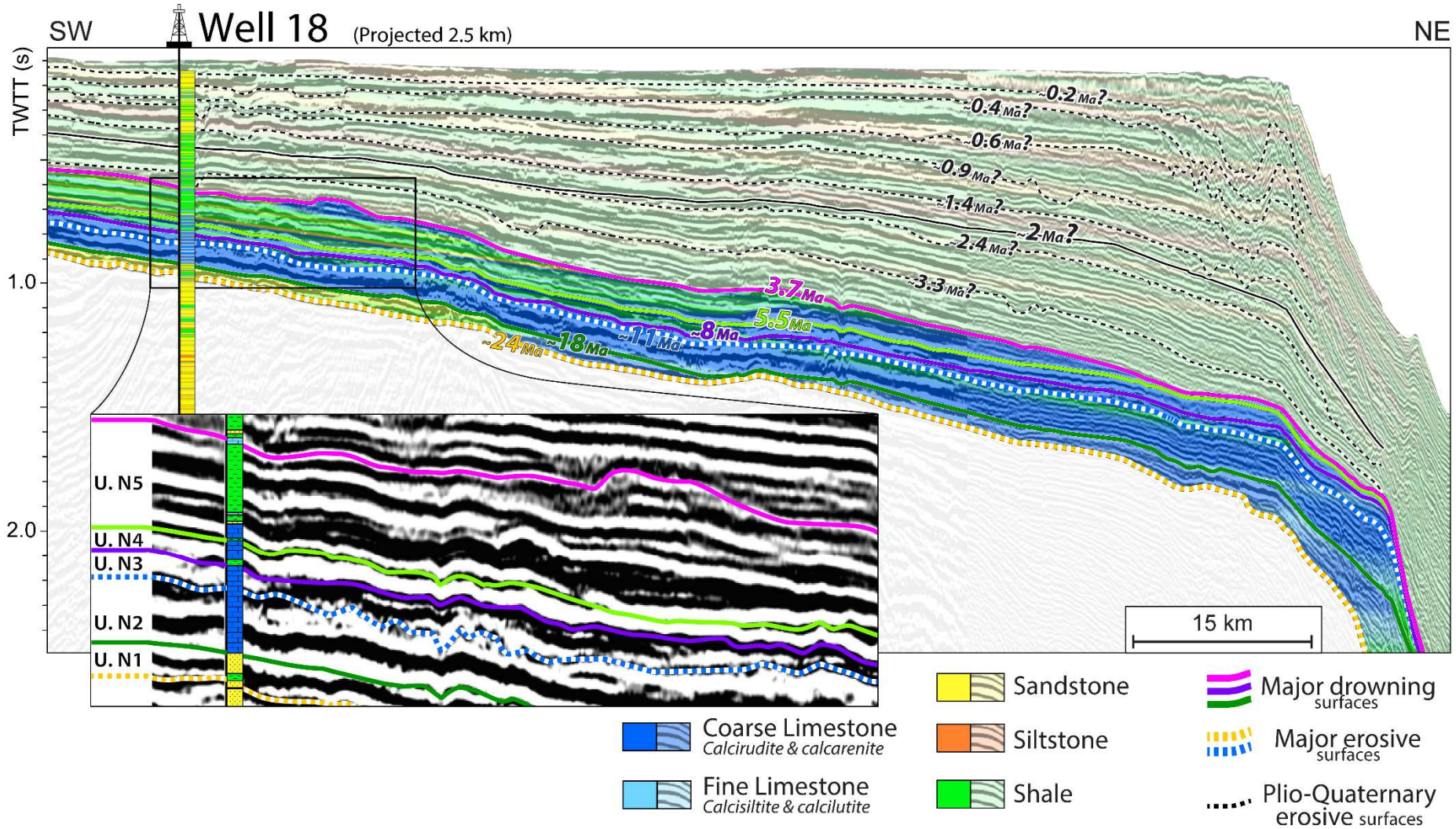

Figure 15: Interpreted seismic profile (location in Figure 1) highlighting each age-constrained surface across the Amazon shelf, together with lithological interpretations based on correlation to well 47B (and neighboring wells). Note that carbonate sedimentation resumed above the ca. 8 Ma Tortonian flooding surface and persisted until the Early Pliocene(unit N5), when a prograding wedge covered the former inner paleo-shelf. Pliocene-Quaternary sequence boundaries after Gorini et al. (2014).

Stage 2 (from ca.8 to 5.5 Ma)

During the deposition of Unit N4 (ca. 8 to 5.5 Ma), the distribution of terrigenous sediments on the Amazon shelf was clearly controlled by the morphology of the former carbonate platform, being mostly confined to inherited topographic lows in the Central and SE shelves (Figs. 13 and 14). The confinement of terrigenous sediments to topographic lows at the top of the carbonate platform was probably caused by a decrease in accommodation space creation in the area during the late Miocene-early Pliocene (quiescent phase in figure 12). Meanwhile, seismic and well data indicate that carbonate production persisted across the NW shelf during the deposition of unit N4 (Fig. 4), confirming that carbonate production persisted for much longer in this area than nearer to the Amazon River mouth as proposed by Gorini et al. (2014). We further argue that carbonate production on the NW shelf was only able to persist during deposition of Unit N4 due to the presence of the large embayment on the Central shelf that captured the Amazon-derived siliciclastic input, virtually isolating the NW shelf from sediments carried by the paleo-Amazon River (Fig. 7).

Stage 3 (from ca. 5.5 to 3.7 Ma)

During the deposition of Unit N5 (early Pliocene), a thick prograding wedge (~85 m) advanced across the inner shelf in the NW region (Fig. 15), showing that the increasing supply of terrigenous sediments was able to circumvent the partially filled embayment on the Central region (Fig. 15). The presence of prograding wedges northwestward of the central embayment indicates that sediments provided by the paleo-Amazon River may have been transported onto the inner shelf by alongshore currents, similarly to what has been reported for the modern NW shelf where sediments transported by the North Brazil Current form prograding subaqueous clinoforms (Nittrouer et al., 1986; Nittrouer et al., 1996). These observations suggest that during the early Pliocene, the entire Amazon shelf was already

subject to conditions comparable to those of the present, with carbonate production greatly reduced due to environmental stresses on carbonate-secreting organisms, such as increasing turbidity and higher nutrient availability leading to eutrophication. This way carbonate sedimentation on the NW shelf was only able to persist only in the form of local buildups on the outer shelf. Such a finding is further supported by a microfacies analysis of samples from wells 18 and 27 (see Figure 1 for locations) by Wolff and Carozzi (1984), who noted that the uppermost units of the carbonate platform represent the first time that bryozoan fragments were the dominant sedimentary components. Although bryozoan fragments are rarely dominant in post-Paleozoic tropical carbonate shelf deposits (Taylor and Allison, 1998), they have been reported to thrive in conditions of limited luminosity and increased nutrient supply (Pomar, 2001). As such, deposition of unit N5 on the NW shelf marks a transition from an environmental context established during the early Miocene (ca. 18 Ma), when carbonate production prevailed across the inner to outer shelf, to the modern depositional pattern in which restricted carbonate sedimentation results in only local thin occurrences, interbedded with upper Pliocene-Quaternary terrigenous successions (Fig. 15).

Stage 4 (3.7 Ma to present)

From 3.7 Ma onwards, siliciclastic sediment supply dominated the Amazon shelf to form prograding clinoforms (Figs. 13-15). Carbonate sedimentation resumed episodically on the outer Amazon shelf during this stage, presumably during periods of reduced terrigenous influx as reported for the last marine transgression (Moura et al., 2016). Nevertheless, the short-lived episodes of sparse carbonate production after 3.7 Ma are not comparable to the earlier widespread carbonate-dominated deposition, which ceased to exist at around 8 Ma on the Central and SE shelf and at 3.7 Ma on the NW shelf.

6. SUMMARY AND CONCLUSIONS

This study provides new insights into the nature and evolution of mixed carbonate-siliciclastic sedimentary succession on the equatorial continental margin offshore the Amazon River, through the correlation of seismically-defined stratigraphic units to lithological and biostratigraphic data in wells. This allows the identification of five Neogene stratigraphic units within the upper Amapá carbonates, the construction of a new age model for their bounding surfaces, and estimates of rates of creation of non-eustatic accommodation space along the shelf. The results also provide new information on the spatial and temporal distribution of carbonate- vs siliciclastic-dominated environments across the shelf during the Neogene, and allow an assessment of the controls on deposition by global sea-level changes and differential subsidence.

One major outcome of this study is to show that the dynamics of mixed carbonate and siliciclastic shelf environments may be strongly influenced by along-shelf variations in accommodation space creation. In the case of the Amazon shelf, this resulted in the development of a 150-km wide embayment on the Central shelf containing greater thicknesses of sediment. Such differential creation of accommodation space, suggested to reflect underlying forms of tectonic subsidence, was the most important factor controlling the distribution and functioning of the carbonate factory during the Neogene.

Another outcome is an alternative model to explain the increased influx of terrigenous sediments into the Offshore Amazon Basin during the late Miocene. We argue that a reduction in the rates of accommodation space creation around 8 Ma may have allowed the progradation of terrigenous depositional systems that were previously being held in proximal positions within the basin. Our results do not exclude the possible establishment of a transcontinental

Amazon River during the late Miocene, but suggest that this may not be necessary to explain the depositional history of the Amazon margin.

Our results also testify to the endurance of carbonate-secreting organisms during the Neogene in equatorial environments, where only large sea-level rises and high terrigenous influxes were able to end regional carbonate production. In this regard, we divided the Amapá carbonates (the Amazon carbonate platform) into three different shelf regions (SE, Central and NW) according to the internal architecture of the carbonate platform. The effects of differential non-eustatic accommodation space creation on the three shelf regions are recognized to have taken place during several main depositional stages:

(1) During a period of increasing accommodation space creation between ca. 18 and 8 Ma, carbonate production grew to dominate the inner parts of the SE and NW shelves as terrigenous sedimentation retreated landward. In contrast, on the Central shelf where the highest rates of accommodation space creation are recorded, carbonate-secreting organisms were unable to keep up with rising sea levels, such that carbonate sedimentation was diminished between ca. 18 and 11 Ma. At ca. 11 Ma a global sea-level fall allowed recolonization of the Central shelf by carbonate-secreting organisms;

(2) A dramatic reduction in accommodation space creation at ca. 8 Ma allowed the progradation of proximal siliciclastic depositional systems, burying carbonates that had previously developed on the SE and Central shelves. Widespread carbonate production was able to persist only on the NW shelf as this area was isolated from the paleo-Amazon River, the sedimentary load of which was captured by the broad embayment on the Central shelf and forced directly to the continental slope;

(3) From 5.5 Ma onwards, the Amazon shelf witnessed another phase of increasing accommodation space creation, probably related to flexural subsidence caused by the

sedimentary load of an increasing sediment influx to the margin. Between ca. 5.5 and 3.7 Ma, sedimentation on the NW shelf underwent a transition from predominantly carbonate to predominantly siliciclastic, as the large embayment on the Central shelf was gradually filled, allowing terrigenous sediment to finally reach the NW shelf. It was only after complete infilling of the central embayment at around 3.7 Ma that terrigenous sediments were able to prograde across the entire NW shelf, leading to cessation of carbonate production on the Amazon continental shelf.

ACKNOWLEDGMENTS

The authors gratefully acknowledge the support granted during the completion of this study by CAPES (Coordination for the Improvement of Higher Level Education- Brazil) in the form of PhD. scholarship made to Alberto M. Cruz and financial support for the project (CAPES-IODP, research grant No. 0558/2015). Antonio Tadeu dos Reis and Cleverson Guizan Silva received research grant No. 313086/2017-6 and No. 308164/2015-6 from the Brazilian National Research Council (CNPq). Daniel Praeg acknowledges funding from the European Union's Horizon 2020 research and innovation program under the Marie Skłodowska-Curie grant agreement No 656821 (global fellowship project SEAGAS), as well as support from CAPES-IODP for a visiting fellowship at UFF. We also acknowledge the Brazilian *Agência Nacional do Petróleo, Gás Natural e Biocombustíveis* (ANP) for seismic and stratigraphic data made available to Universidade Federal Fluminense (UFF) and Universidade do Estado de Rio de Janeiro (UERJ). Our special thanks are also due to CGG, GAIA and FUGRO for making additional seismic data available and for permission to publish our results, to the Brazilian Navy (DHN/LEPLAC- The Brazilian Continental Shelf Survey

Programme) for permission to use the LEPLAC seismic lines, and to SMT Kingdom for the use of educational licenses of the software Kingdom Suite®.

Finally, we would like to thank for all the suggestions and corrections made during the review process. Special thanks to Dr. André Strasser for his critical and insightful comments that much improved the overall quality of this manuscript. We also thank Alexandre Lethier for diligently drafting all the figures included in this paper. This is a contribution of the research group GEOMARGEM: Geology and Oceanography of Passive Continental Margins (http://www.geomargem.org).

7. REFERENCES

Allen, P.A., and Allen, J.R., 2005, Basin analysis. Principles and applications: Blackwell Science, Oxford, UK.

Anthonissen, D.E., and Ogg, J.G., 2012, Appendix 3 - Cenozoic and Cretaceous Biochronology of Planktonic Foraminifera and Calcareous Nannofossils: The Geologic Time Scale, v. 27, no. June 2011, p. 1083–1127, doi: http://dx.doi.org/10.1016/B978-0-444-59425-9.15003-6.

Betzler, C., Furstenau, J., Ludmann, T., Hubscher, C., Lindhorst, S., Paul, A., Reijmer, J.J.G., and Droxler, A.W., 2013, Sea-level and ocean-current control on carbonate-platform growth, Maldives, Indian Ocean: Basin Research, v. 25, no. 2, p. 172–196, doi: 10.1111/j.1365-2117.2012.00554.x.

Braga, S., 1993, Resposta flexural da litosfera e subsidência regional na área do Cone do Amazonas: Boletim de Geociências da Petrobras, v. 7, no. 1, p. 157–172.

Brandão, J.A.S.L., and Feijó, F.J., 1994, Bacia da Foz do Amazonas: Boletim de Geociências da Petrobras, v. 8, no. 1, p. 91–99.

Bukry, D., 1973. Low-latitude coccolith biostratigraphic zonation. *In* Edgar, N.T., Saunders, J.B., et al., *Init. Repts. DSDP*,15: Washington (U.S. Govt. Printing Office), 685-703

Burgess, P.M., Winefield, P., Minzoni, M., and Elders, C., 2013, Methods for identification of isolated carbonate buildups from seismic reflection data: AAPG Bulletin, doi: 10.1306/12051212011.

Campbell, K.E., 2010, Late Miocene onset of the Amazon River and the Amazon deep-sea fan: Evidence from the Foz do Amazonas Basin: COMMENT: Geology, v. 38, no. 7, p. e212, doi: 10.1130/G30633C.1.

Campbell, K.E., Frailey, C.D., and Romero-Pittman, L., 2006, The Pan-Amazonian Ucayali

Peneplain, late Neogene sedimentation in Amazonia, and the birth of the modern Amazon River system: Palaeogeography, Palaeoclimatology, Palaeoecology, v. 239, no. 1–2, p. 166–219, doi: 10.1016/j.palaeo.2006.01.020.

Carozzi, a V, 1981, Porosity models and oil exploration of Ampa carbonates, Paleogene, Foz do Amazonas Basin, offshore NW Brazil: Journal of Petroleum Geology, v. 4, no. 1, p. 3–34.

Castro, J.C. de, Miura, K., and Braga, J.A.E., 1978, Stratigraphic and Structural Framework of the Foz do Amazonas Basin, *in* 10th Annual Offshore Technology Conference, Offshore Technology Conference, Houston, Texas, p. 1843–1847.

Catuneanu, O., 2002, Sequence stratigraphy of clastic systems: Concepts, merits, and pitfalls: Journal of African Earth Sciences, v. 35, no. 1, p. 1–43.

Cobbold, P.R., Mourgues, R., and Boyd, K., 2004, Mechanism of thin-skinned detachment in the Amazon Fan: Assessing the importance of fluid overpressure and hydrocarbon generation: Marine and Petroleum Geology, v. 21, no. 8, p. 1013–1025, doi: 10.1016/j.marpetgeo.2004.05.003.

Cruz, A.M., Gorini, C., Reis, A.T., Haq, B., Silva, C.G., and Granjeon, D., 2014, Integrated geological, geophysical and numerical modeling studies applied to the understanding of Amazon River Mouth Basin evolution, *in* 19th ISC, Geneva; Switzerland, p. 166.

Damuth, J.E., Kowsmann, R.O., Flood, R.D., Belderson, R.H., and Gorini, M.A., 1983, Age relationships of distributary channels on Amazon deep-sea fan: implications for fan growth pattern.: Geology, v. 11, no. 8, p. 470–473.

Damuth, J.E., and Kumar, N., 1975, Amazon Cone: Morphology, Sediments, Age, and Growth Pattern: Bulletin of the Geological Society of America, v. 86, no. 6, p. 863–878.

Dobson, D.M., Dickens, G.R., and Rea, D.K., 2001, Terrigenous sediment on Ceara Rise: A Cenozoic record of South American orogeny and erosion: Palaeogeography, Palaeoclimatology, Palaeoecology, v. 165, no. 3–4, p. 215–229.

Driscoll, N.W., and Karner, G.D., 1994, Flexural deformation due to Amazon Fan loading: a feedback mechanism affecting sediment delivery to margins: Geology, v. 22, no. 11, p. 1015–1018, doi: 10.1130/0091-7613(1994)022<1015:FDDTAF>2.3.CO;2.

Figueiredo, J., Hoorn, C., van der Ven, P., and Soares, E., 2009, Late Miocene onset of the Amazon River and the Amazon deep-sea fan: Evidence from the Foz do Amazonas Basin: Geology, v. 37, no. 7, p. 619–622.

Figueiredo, J., Hoorn, C., van der Ven, P., and Soares, E., 2010, Late Miocene onset of the Amazon River and the Amazon deep-sea fan: Evidence from the Foz do Amazonas Basin: Reply: Geology, v. 38, no. 7, p. e213, doi: 10.1130/G31057Y.1.

Figueiredo, J.J.P., Zalán, P.V., and Soares, E.F., 2007, Bacia da Foz do Amazonas: Boletim de Geociencias da Petrobras, v. 15, no. 2, p. 299–309.

Gorini, C., Haq, B.U., dos Reis, A.T., Silva, C.G., Cruz, A.M., Soares, E., and Grangeon, D., 2014, Late Neogene sequence stratigraphic evolution of the Foz do Amazonas Basin, Brazil: Terra Nova, v. 26, no. 3, p. 179–185, doi: 10.1111/ter.12083.

Gradstein, F.M., Ogg, J.G. and Smith, A.G., 2004, A Geologic Time Scale (F.M.Gradstein, J.G. Ogg, & Smith, A.G., Eds.). Cambridge University Press, Cambridge.

Gradstein, F.M., Ogg, J.G., Schmitz, M.D., and Ogg, G.M., 2012, The Geologic Time Scale (F. M. Gradstein, J. G. Ogg, M. D. Schmitz, & G. M. Ogg, Eds.): Elsevier B.V., Amsterdam.

Handford, C.R., and Loucks, R.G., 1993, Carbonate depositional sequences and systems tracts—responses of carbonate platforms to relative sea-level change, *in* Carbonate Sequence Stratigraphy; Recent Advances and Applications: AAPG Memoir 57, p. 3–41.

Haq, B.U., Hardenbol, J., and Vail, P.R., 1987, Chronology of fluctuating sea levels since the triassic.: Science (New York, N.Y.), v. 235, no. 4793, p. 1156–1167.

Hoorn, C., Bogotá-A, G.R., Romero-Baez, M., Lammertsma, E.I., Flantua, S.G.A., Dantas, E.L., Dino, R., do Carmo, D.A., and Chemale, F., 2017, The Amazon at sea: Onset and stages of the Amazon River from a marine record, with special reference to Neogene plant turnover in the drainage basin: Global and Planetary Change, v. 153, p. 51–65, doi: 10.1016/j.gloplacha.2017.02.005.

Latrubesse, E., Cozzuol, M., Silva-Caminha, S., Rigsby, C., Absy, M., and Jaramillo, C., 2010, The Late Miocene paleogeography of the Amazon Basin and the evolution of the Amazon River system: Earth-Science Reviews, v. 99, no. 3–4, p. 99–124, doi: 10.1016/j.earscirev.2010.02.005.

Martini, E., 1971, Standard Tertiary and Quaternary calcareous nannoplankton zonation: Conf. Planktonic Microfossils Roma, v. 2, p. 739–785.

Matos, R.M.D. De, 2000, Tectonic Evolution of the Equatorial South Atlantic: Atlantic Rift and Continental Margins, v. 115, p. 331–354, doi: 10.1029/GM115p0331.

Miller, K.G., Kominz, M. a., Browning, J. V., Wright, J.D., Mountain, G.S., Katz, M.E., Sugarman, P.J., Cramer, B.S., Christie-Blick, N., and Pekar, S.F., 2005, The Phanerozoic record of sea-level change: Science, v. 310, no. 5752, p. 11293–1298, doi: 10.1126/science.1116412.

Mitchum, R.M., and Vail, P.R., 1977, Seismic Stratigraphy and Global Changes of Sea Level , Part 7 : Seismic Stratigraphic Interpretation Procedure: Seismic Stratigraphy: Applications to Hydrocarbon Exploration. AAPG Memoir 26, v. Memoir 26, p. 135–143.

Moura, R.L., Amado-Filho, G.M., Moraes, F.C., Brasileiro, P.S., Salomon, P.S., Mahiques, M.M., Bastos, A.C., Almeida, M.G., Silva, J.M., Araujo, B.F., Brito, F.P., Rangel, T.P., Oliveira, B.C.V., Bahia, R.G., Paranhos, R.P., Dias, R.J.S., Siegle, E., Figueiredo, A.G., Pereira, R.C., Leal, C. V., Hajdu, E., Asp, N.E., Gregoracci, G.B., Neumann-Leitão, S., Yager, P.L., Francini-Filho, R.B., Fróes, A., Campeão, M., Silva, B.S., Moreira, A.P.B., Oliveira, L., Soares, A.C., Araujo, L., Oliveira, N.L., Teixeira, J.B., Valle, R.A.B., Thompson, C.C., Rezende, C.E. and Thompson, F.L., 2016. An extensive reef system at the Amazon River mouth:Science advances, 2, p. 1–11, doi: 10.1126/sciadv.1501252.

Nittrouer, C. a., Kuehl, S. A., Figueiredo, A.G., Allison, M. A., Sommerfield, C.K., Rine, J.M., Faria, L.E.C., and Silveira, O.M., 1996, The geological record preserved by Amazon shelf sedimentation: Continental Shelf Research, v. 16, no. 5–6, p. 817–841.

Nittrouer, C.A., Kuehl, S.A., Demaster, D.J., and Kowsmann, R.O., 1986, The deltaic nature of Amazon shelf sedimentation.: Geological Society of America Bulletin, doi: 10.1130/0016-7606(1986)97<444:TDNOAS>2.0.CO;2.

Nogueira, A.C.R., Silveira, R., and Guimarães, J.T.F., 2013, Neogene-Quaternary

sedimentary and paleovegetation history of the eastern Solimões Basin, central Amazon region: Journal of South American Earth Sciences, v. 46, p. 89–99, doi: 10.1016/j.jsames.2013.05.004.

Perovano, R., Reis, A.T. dos, Silva, C.G., Vendeville, B.C., Gorini, C., Oliveira, V. De, and Araújo, É.F. da S., 2009, O Processo de Colapso Gravitacional da Seção Marinha da Bacia da Foz do Amazonas - Margem Equatorial Brasileira: Revista Brasileira de Geofíca, v. 27, no. 3, p. 459–484.

Pomar, L., 2001, Types of carbonate platforms: A genetic approach: Basin Research, doi: 10.1046/j.0950-091X.2001.00152.x.

Raffi, I., Backman, J., Fornaciari, E., Pälike, H., Rio, D., Lourens, L., and Hilgen, F., 2006, A review of calcareous nannofossil astrobiochronology encompassing the past 25 million years: Quaternary Science Reviews, v. 25, no. 23–24, p. 3113–3137, doi: 10.1016/j.quascirev.2006.07.007.

Reis, A.T., Araújo, E., Silva, C.G., Cruz, A.M., Gorini, C., Droz, L., Migeon, S., Perovano, R., King, I., and Bache, F., 2016, Effects of a regional décollement level for gravity tectonics on late Neogene to recent large-scale slope instabilities in the Foz do Amazonas Basin, Brazil: Marine and Petroleum Geology, doi: 10.1016/j.marpetgeo.2016.04.011.

Reis, a. T., Perovano, R., Silva, C.G., Vendeville, B.C., Araujo, E., Gorini, C., and Oliveira, V., 2010, Two-scale gravitational collapse in the Amazon Fan: a coupled system of gravity tectonics and mass-transport processes: Journal of the Geological Society, v. 167, no. 3, p. 593–604, doi: 10.1144/0016-76492009-035.

Rodger, M., Watts, a. B., Greenroyd, C.J., Peirce, C., and Hobbs, R.W., 2006, Evidence for unusually thin oceanic crust and strong mantle beneath the Amazon Fan: Geology, v. 34, no. 12, p. 1081, doi: 10.1130/G22966A.1.

Schaller, H., Vasconcelos, D.N., and Castro, J.C., 1971, Estratigrafia preliminar da Bacia Sedimentar da Foz do Rio Amazonas, *in* XXV Congresso Brasileiro de Geologia, SBG, São Paulo, p. 189–202.

Schlager, W., 1998, Exposure, Drowning and Sequence Boundaries on Carbonate Platforms, *in* Camoin, G.F. and Davies, P.J. eds., Reefs and Carbonate Platforms in the Pacific and Indian Oceans, Blackwell Publishing Ltd., Oxford, UK, p. 3–21.

Schlager, W., 2005, Geometry of carbonate accumulations, *in* Crossey, L.J. ed., Carbonate Sedimentology and Sequence Stratigraphy, SEPM (Society for Sedimentary Geology), Tulsa, Oklahoma, p. 39–54.

Schlager, W., John, J.G.R., and Droxler, A.W., 1994, Highstand Shedding of Carbonate Platforms: SEPM Journal of Sedimentary Research, doi: 10.1306/D4267FAA-2B26-11D7-8648000102C1865D.

Silva, G.G., Araujo, E., Reis, A.T., Perovano, R., Gorini, C., Vendeville, B.C., and Albuquerque, N., 2010, Megaslides in the Foz do Amazonas Basin, Brazilian Equatorial Margin (D. C. Mosher, C. Shipp, L. Moscardelli, J. Chaytor, C. Baxter, H. Lee, & R. Urgeles, Eds.): Submarine Mass Movements and Their Consequences, v. 28, no. 46, p. 581–591.

Silva, S.R.P., Maciel, R.R., and Severino, M.C.G., 1999, Cenozoic tectonics of Amazon Mouth Basin: Geo-Marine Letters, v. 18, no. 3, p. 256–262.

Silva, C.C., Reis, A.T. dos, Perovano, R.J., Gorini, M.A., Santos, M.V.M. dos, Jeck, I.K., Tavares, A.A.A., and Gorini, C., 2016, Multiple Megaslide Complexes and Their Significance for the Miocene Stratigraphic Evolution of the Offshore Amazon Basin, *in* Lamarche, G., Mountjoy, J., Bull, S., Hubble, T., Krastel, S., Lane, E., Micallef, A., Moscardelli, L., Mueller, C., Pecher, I., and Woelz, S. eds., Advances in Natural and Technological Hazards Research, p. 49–60.

Taylor, P.D., and Allison, P.A., 1998, Bryozoan carbonates through time and space: Geology, doi: 10.1130/0091-7613(1998)026<0459:BCTTAS>2.3.CO.

Vail, P.R., Mitchum, R.M., and Thompson, S., 1977, Seismic Stratigraphy and Global Change in Sea Level, Part 3: Relative Change af Sea Level from Coastal Onlap: In Payton, C.E. (ed.) Seismic Stratigraphy – Applications to Hydrocarbon Exploration, American Association of Petroleum Geologists, v. Memoir 26, p. 63–81.

Wolff, B., and Carozzi, A.V., 1984, Microfacies, depositional environments, and diagenesis of the Amapá carbonates (Paleocene-Middle Miocene), Foz do Amazonas basin, offshore NE Brazil: Petrobras, Rio de Janeiro.

Woolfe, K.J., and Larcombe, P., 1998, Terrigenous sediment accumulation as a regional control on the distribution of reef carbonates, *in* Reefs and Carbonate Platforms in the Pacific and Indian Oceans,.

Young, J.R., 1998, Neogene, *in* Bown, P.. ed., Calcareous Nannofossil Biostratigraphy, British Micropalaeontological Society Publications Series, London, p. 225–265.

Zeeden, C., Hilgen, F., Westerhold, T., Lourens, L., Röhl, U., and Bickert, T., 2013, Revised Miocene splice, astronomical tuning and calcareous plankton biochronology of ODP Site 926 between 5 and 14.4Ma: Palaeogeography, Palaeoclimatology, Palaeoecology, v. 369, p. 430–451.

HIGHLIGHTS

(1) New age models allow to clarify the Neogene history of the Amazon shelfal carbonates

(2) Differential subsidence strongly controls shelf architecture between ca. 24-3,7Ma

(3) Higher siliciclastic influx suppressed the Central and NW shelf carbonates at ca. 8Ma

(4) Carbonate production locally persisted on the NW Amazon shelf until ca. 3.7Ma

(5) Reduction of regional subsidence rates led to the death of shelfal carbonates